Local Glutamate-Mediated Dendritic Plateau Potentials Change the State of the Cortical Pyramidal Neuron

Abbreviated title: *Glutamate-Mediated Dendritic and Somatic Plateaus*

[a]Peng P. GAO, [b]Joseph. W. GRAHAM, [a]Wen-Liang ZHOU, [a]Jinyoung JANG, [b]Sergio ANGULO, [b]Salvador DURA-BERNAL, [d]Michael HINES, [b,c]William W. LYTTON and [a]Srdjan D. ANTIC*

[a] Institute for Systems Genomics, UConn Health, Farmington, CT, USA
[b] Physiology & Pharmacology, SUNY Downstate, Brooklyn, NY, USA
[c] Kings County Hospital, Brooklyn, NY, USA
[d] Department of Neuroscience, Yale University, New Haven, CT, USA

Corresponding author:
Srdjan D. Antic, UConn Health School of Medicine, 263 Farmington Ave., Farmington, CT, 06030, antic@uchc.edu

Acknowledgements:
We are grateful to Corey Acker and Guy Major for providing their model code, to Chun Bleau (Redshirt Imaging) and Charlie Bleau (SciMeasure Analytical Systems) for assistance with imaging equipment. This work was supported by National Institute of Mental Health, R01MH063503, U01MH109091 and R01MH086638; National Institute of Neural Disorders and Stroke, R01NS11613; National Institute of Biomedical Imaging and Bioengineering, R01EB022903 and U01EB017695.

Author Contributions:
M.H., W.W.L., and S.D.A. designed the research; P.P.G., J.W.G., W.L.Z., J.J., S.A., and S.D.B. designed and performed experiments and simulations; P.P.G., J.W.G., and S.D.A. analyzed the data. The paper was written by P.P.G., M.H., W.W.L., and S.D.A., with input from all of the authors.

Competing Interests:
The authors declare no competing financial interests.

Abstract

Dendritic spikes in thin dendritic branches (basal and oblique dendrites) of pyramidal neurons are traditionally inferred from spikelets measured in the cell body. Here, we used laser-spot voltage-sensitive dye imaging in cortical pyramidal neurons (rat brain slices) to investigate the voltage waveforms of dendritic potentials occurring in response to spatially-restricted glutamatergic inputs. Local dendritic potentials lasted 200–500 ms and propagated to the cell body where they caused sustained 10-20 mV depolarizations. Plateau potentials propagating from dendrite to soma, and action potentials propagating from soma to dendrite, created complex voltage waveforms in the middle of the thin basal dendrite, comprised of local sodium spikelets, local plateau potentials, and back-propagating action potentials, superimposed on each other. Our model replicated these experimental observations and made the following predictions: (i) membrane time constant is shortened during the plateau; and (ii) synaptic responses are more effective drivers of neuronal action potentials during the plateau potential. Dendritic plateau potentials occurring in basal and oblique branches put pyramidal neurons into an activated neuronal state ("prepared state"), characterized by depolarized membrane potential and notably faster membrane responses. The prepared state provides a time window of 200-500 ms during which cortical neurons are particularly excitable and capable of following afferent inputs. At the network level, this predicts that sets of cells with simultaneous plateaus would provide cellular substrate for the formation of functional neuronal ensembles.

Key words: nonlinear, integration, NMDA spike, ensembles, membrane time constant

Significance statement: Strong and clustered glutamatergic inputs will have a major influence on activity at both neuronal and network scales. We recorded glutamate-mediated dendritic voltage plateaus using voltage imaging, and created a computer model that recreated experimental measures. Our model predicts the manner in which plateaus are triggered and the impact of inputs to an individual thin dendrite on the membrane response in the cell body. Plateau potentials profoundly change neuronal state -- a plateau potential triggered in one basal dendrite depolarizes the soma and shortens membrane time constant, making the cell more susceptible to firing triggered by other afferent inputs. We tested model predictions experimentally.

Introduction

The individual spiny neuron is subjected to a variety of excitatory input patterns, often resulting from concurrent release across multiple synapses on a single dendrite. Due to combinations of temporal and spatial clustering[1-3], the amount of glutamate released on a single basilar dendrite can be quite large, potentially spilling over to extrasynaptic NMDA receptors, and temporarily overwhelming the ability of astrocytes to fully compensate. *In vitro* focal applications of comparable amounts of glutamate, or repetitive synaptic stimulations, will trigger dendritic plateau potentials in dendrites of CNS spiny neurons[4-9]. Originally demonstrated *in vitro*, dendritic plateau potentials have now been demonstrated *in vivo* as well[10-16]. Glutamate-mediated dendritic spikes underlie synaptic plasticity, sensory processing, and behavior[10,14,17,18]. Studying the biophysical aspects of dendritic plateau potentials entails experimental measurements of precise dendritic voltage waveforms along basal, oblique and tuft dendrites. These cannot be obtained using patch electrodes, since it is not yet possible to consistently get multiple electrodes onto a single thin branch[19,20].

NMDA spikes have been recorded by a number of groups and have been replicated computationally[21-24]. By contrast, glutamate-mediated plateaus are less fully explored, and less well understood. In this paper, we analyze properties and mechanisms of dendritic plateaus through coupled experimentation and computer simulation. New experimental measurements in dendrites of cortical pyramidal neurons were used to create a detailed computational model of dendritic plateaus in a full morphology model of a Layer 5 cortical pyramidal cell, demonstrating that the dynamics of these potentials will have a major effect on spike generation: the plateau not only places the cell closer to spike threshold but also shortens the membrane time constant. As a consequence, other incoming excitatory postsynaptic potentials (EPSPs), arriving on other dendritic branches, become much more potent drivers of action potential (AP) initiation during the plateau event. The results from the detailed model support a working hypothesis that plateau potentials would allow cortical pyramidal neurons to respond quickly to ongoing network activity and potentially enable synchronized firing to form active neural ensembles[25-27].

Methods and Materials

Brain slice and electrophysiology

Sprague Dawley rats (P21 – 42) of both sexes were anesthetized with isoflurane, decapitated, and the brains were removed with the head immersed in ice-cold, artificial cerebrospinal fluid (ACSF), according to an institutionally approved animal protocol. ACSF contained (in mM) 125 NaCl, 26 $NaHCO_3$, 10 glucose, 2.3 KCl, 1.26 KH_2PO_4, 2 $CaCl_2$ and 1 $MgSO_4$, at pH 7.4. Coronal slices (300 µm) were cut from frontal lobes. Whole-cell recordings were made from visually identified layer 5 pyramidal neurons. Intracellular solution contained (in mM) 135 K-gluconate, 2 $MgCl_2$, 3 Na_2-ATP, 10 Na_2-phosphocreatine, 0.3 Na_2-GTP and 10 Hepes (pH 7.3, adjusted with KOH). In some experiments, the intracellular solution was enriched with the fluorescent dye Alexa Fluor 594 (40 µM) to aid positioning of glutamate stimulation electrodes on distal dendritic branches. Electrical signals were amplified with a Multiclamp 700A and digitized with two input boards: (1) Digidata Series 1322A (Molecular Devices, Union City, CA) at 5 kHz, and (2) Neuroplex (RedShirtImaging, Decatur, GA) at 2.7 kHz sampling rate. All experiments were performed at 33-34°C. Glutamate microiontophoresis was performed using sharp pipettes (40 ± 10 MΩ) pulled from borosilicate glass with filament (1.5 mm OD), and backfilled with 200 mM Na-glutamate (pH=9). A programmable stimulator (Clampex, Molecular Probes) and stimulus isolation unit IsoFlex (A.M.P.I.) were used to iontophoretically eject glutamate. A motorized micromanipulator Shutter M-285 was used to drive the tips of glutamate pipettes into the slice tissue with both “X” and “Z” axis motors engaged simultaneously. This was done to prevent bending of the sharp electrode, which occurs if a simple “Z” axis motion is used.

Dye Injections

The voltage-sensitive dye injection protocol was previously described in[28]. Briefly, neurons were filled through whole-cell recording pipettes with a styryl voltage-sensitive dye JPW3028 (Potentiometric Probes, Farmington, CT) dissolved in standard K-gluconate based intracellular solution. Dye loading patch pipettes were filled with two varieties of the same intracellular solution; one with and one without the dye. Dye-free solution occupied the very tip of the pipette, while the back of the pipette lumen was microloaded with dye-rich solution (400 – 800 µM). The purpose of dye-free solution in the tip of the patch pipette was to prevent dye-leak during the maneuver through brain slice tissue. JPW3028 is lipophilic and binds indiscriminately and irreversibly to all membranes. Even a small amount of dye leak during the formation of the gigaohm seal can generate strong fluorescent background, which has a devastating effect on

dendritic optical signals. The filling pipette was carefully pulled out (outside-out patch) and brain slices were left to incubate for 40-120 minutes at room temperature. Just before optical recordings, the cells were re-patched with dye-free pipette at physiological temperature (33-34°C).

Dendritic voltage imaging

Voltage-sensitive dye imaging was performed on a Zeiss Axioskope 2FS microscope equipped with NeuroCCD camera (RedShirtImaging). We used Zeiss 40X objective IR-Achroplan 0.80 NA. Laser spot illumination was used to excite the voltage-sensitive dye[29]. Into the epi-illumination port of the microscope, we inserted a Φ200 µm fiber optic guide with a collimator. The laser beam (Cobolt Samba 532 nm, 150 mW) was focused on the other side of the fiber optic guide using a microscope objective lens. This arrangement produced a motionless spot of laser light (25 - 50 µm in diameter) at the object plane. A region of interest (ROI) was brought into the laser spot using X-Y microscope platform. The laser beam was interrupted by an electro-programmable shutter (Uniblitz, Vincent Associates). Laser beams were directed onto the preparation with the help of Zeiss epi-illumination filter cube: exciter 520 ± 45 nm; dichroic 570 nm; emission >610 nm.

Optical signals were recorded with 80 x 80 pixels at a 2.7 kHz frame rate, stored, and then temporally filtered (off-line) with digital Gaussian low-pass filter (1050 Hz cut-off), and Butterworth high-pass filter (4.5 Hz), unless otherwise specified. To improve signal-to-noise ratio several pixels (3 – 8 pixels) were selected inside the region of interest and spatially averaged, unless otherwise specified. With the 40X magnification lens, used in this study, each pixel covers 4.8 x 4.8 µm in the object field. After the experiment, fluorescent images were captured with IR-1000 Dage CCD camera. In order to obtain whole-field photographs of the dendritic tree, brain slices were removed from the recording chamber and mounted on a microscope slide in water-based mounting medium. Mounted microscope slides were transferred to Zeiss Axiovert200M imaging station where photographs were taken with AxioVision LE system using 20x dry and 40x oil immersion objectives.

Physiology data analysis

Optical and electrical measurements were analyzed using the software Neuroplex (RedShirtImaging) and Clampfit (Molecular Probes). Plateau amplitude was measured as a difference between the peak depolarization after the last AP in the burst and the baseline. Duration of the plateau depolarization was measured at 50% of plateau amplitude. The linear

correlation coefficient (c.c.) and graph plotting were done in custom made software written in Python. The backpropagation action potential (bAP) amplitude atop plateaus was measured from the plateau phase ('p') to the peak of APs. The amplitude of the test-pulse-evoked voltage transients (ΔVm) was measured as a difference between voltage transient peak and baseline established just prior to current injection (plateau level). Membrane time constant (TAU) was measured in Clampfit by fitting an exponential through the charging curve.

Modeling

The simulations were implemented with the NEURON simulator (version 7.5)[30] through its Python interface (version 2.7). The full model is available from ModelDB (accession number 249705). Here briefly, the multi-compartment cell was modified from a morphologically detailed L5 pyramidal neuron[31]. It has 85 compartments and 439 segments in total: 36 compartments for basal dendrites, 45 for apical dendrites, 3 for soma and 1 for axon.

The detailed channel parameters are listed in Table 1.

Table 1			
Channels	Conductance	Units	Ref
Voltage-gated sodium channels		pS/μm^2	31 32
- Soma	900		
- Basal dendrite	150 - distance*0.5		
- Apical dendrite	375		
- Axon	150		
- AIS	5,000		
A-type potassium channels		pS/μm^2	31,33
- Soma	150		
- Basal dendrite	Distal (150 + 0.7*distance) * (1/300*distance) Proximal (150 + 0.7*distance) * (1 - 1/300*distance)		
- Apical dendrite	Distal 300* (1/300*distance) Proximal 300* (1 - 1/300*distance)		
High voltage activated calcium		pS/μm^2	31,32,34

channels			
- Soma	2		
- Basal dendrite	Distal 0.4 Proximal 2		
- Apical dendrite	Distal 0.4 Proximal 2		
Low voltage activated calcium channels		pS/μm^2	31,32,34
- Soma	2		
- Basal dendrite	Distal 1.6 Proximal 2		
- Apical dendrite	Distal 1.6 Proximal 2		
HCN channels		S/cm2	35
- Soma	0.0001		
- Basal dendrite	0.0001		
- Apical dendrite	0.0002*(-0.8696 + 2.0870*exp(distance/323))		
Calcium activated potassium channels	2.68e-4	S/cm2	36,37
Kv channel		pS/μm2	31,32
- Soma	40		
- Basal dendrite	40		
- Apical dendrite	40		
- Axon	100		

Table 1. Model parameters.

Modeling bAPs

We investigated the properties of bAPs on 6 different basal branches using similar methods as [31]. Square waveform current pulses (3 nA, 1.75 ms) ware injected in the soma; and the spike amplitude and peak time were measured at different locations along 6 basal dendrites. For TTX and 4-AP conditions, the sodium channel or A-type potassium channel conductances were set to 0, respectively. The binned average (bin size = 20 μm) spike amplitude and peak latency were plotted against the location on basal dendrites, as the distance from soma.

Modeling glutamate inputs

The glutamate microiontophoresis experiments were simulated by activation of AMPA and NMDA receptor models. AMPA and NMDA receptors were activated within a dendritic segment

(~60 µm length) on the targeted basal dendrite. The proximal edge of the activated dendritic segment was 70 µm away from the soma. In order to study the effect of input location and the spatial profile in dendrites, the length of the active dendritic segments was decreased to 10 - 30 µm.

Glutamate receptor channels were divided into two groups: synaptic (AMPA and NMDA, ratio 1:1); and extrasynaptic (NMDA). The ratio of synaptic to extrasynaptic NMDA conductance was set at 1:1. The extrasynaptic NMDA receptors were always activated 5 ms after the activation of the neighboring synaptic NMDA receptors. The glutamate input strength was regulated through a "weight factor", which simultaneously scaled three parameters: [1] the number of activated receptors; [2] the synaptic weights; and [3] the receptor activation time window. The minimum receptor activation time window was 40 ms when the weight factor was set to 0, and the maximum time window was 90 ms, when the weight factor was equal to 1. Two types of temporal activation patterns were used: [1] the random function (continuous uniform distribution) and [2] the beta random function, available in the Python NumPy library. Two membrane mechanisms for NMDAr were used, resulting in two cell models: [Model 1] the classical two state kinetic model with alpha – function[38]; and [Model 2] the triple-exponential "envelope" time course and a sigmoidal voltage dependence[6]. The same AMPA receptors were used in Models 1 & 2[38]. In all simulations, the maximum conductances (g_max) for AMPA, synaptic NMDA and extrasynaptic NMDA were 0.05 µS, 0.005 µS, and 0.005 µS, respectively. Barrages of EPSPs were simulated as the activation of AMPA receptors only on 5 dendritic branches, different from the dendritic branch receiving glutamate input for initiation of local plateau potential.

Quantifications of the modeling results

The measurements of plateau amplitude, duration and spikes per plateau in both experiments and simulations were implemented using Python. Plateau amplitude was calculated as the minimum voltage value between the last two APs riding on top of the plateau potential. Plateau duration was calculated as the period of time during which the voltage was higher than the half plateau amplitude (half-width). The membrane time constant was measured in response to a square wave current injection, as the time required for decaying to 37% of its initial value. Local input resistance in dendrites was attained by injecting a standard current pulse (100 pA, 100 ms) and measuring local ΔVm.

Results

We simultaneously recorded dendritic and somatic potentials in 10 layer V pyramidal neurons, with somatic recordings alone in an additional 15 cells. Simulation fitting was done by hand in a single full multicompartment morphology over several thousand simulation runs.

I Experiment: glutamate-evoked dendritic plateau potentials

Plateau potentials were induced by brief (5 ms) pulses of iontophoretically ejected glutamate applied locally on individual dendrites of cortical Layer 5 pyramidal neurons (**Fig. 1A$_1$**, glut.). Voltage waveforms of plateau potentials in basal and oblique dendrites were recorded with voltage-sensitive dye imaging (**Fig. 1A$_2$**, dend.). Simultaneously with dendritic voltage imaging, we recorded somatic membrane potential in whole-cell (**Fig. 1A$_2$**, soma).

Glutamate threshold. The glutamate pulse invariably produced a dendritic depolarization (**Fig. 1AB**) in all neurons tested in this way (n = 10). At lower glutamate input intensities, the depolarization was seen as a brief EPSP (**Fig. 1A$_2$**, gray traces). As the intensity of the glutamatergic stimulation was gradually increased in equal steps (~10 nA, intensity of iontophoretic current) a threshold was reached with a discontinuity from small EPSP depolarizations up to the plateau voltage level. The passage from subthreshold (**Fig. 1AB**, dark blue trace) to suprathreshold (red trace), could be seen in both dendrite and soma. Further increase in glutamate input intensity did not result in greater depolarization, but prolonged the duration of the plateau (**Fig. 1AB**, orange traces), suggesting an all-or-none spike mechanism[39].

Voltage waveform at the input site. Locally, dendritic plateaus showed a characteristic voltage waveform (**Fig. 1C),** beginning with a rapid onset ('r'). The sudden increase in voltage, seen clearly in the dendrite, was low-pass filtered by the dendritic cable and so appeared less abrupt in the soma (**Fig. 1C**, soma). This onset phase was capped with an initial sodium spikelet ('s'), described further below. The dendritic plateau phase ('p') lasted >100 ms but terminated with an abrupt decline, or collapse ('c') back to resting potential.

Collision of 3 spikes in mid dendrite. Simultaneous recordings from 2 dendritic sites (**Fig. 1D$_1$**) revealed three spikes varieties including: [1] square-shaped glutamate-mediated dendritic plateau potentials (**Fig. 1D$_2$**, red trace); [2] dendrite-originating fast sodium spikes uncoupled

from somatic APs (**Fig. 1D$_3$**, "*init. s*"); and [3] fast sodium spikes associated with firing of APs in the cell body – backpropagating APs (**Fig. 1D$_3$**, "*bAPs*"). The most distal dendritic segment, closest to the point of glutamatergic input was dominated by square-shaped plateau potentials (**Fig. 1D$_{2\text{-}3}$**, red traces). The cell body was dominated by APs (**Fig. 1D$_{2\text{-}3}$**, black traces). The mid dendritic segment experienced a complex voltage waveform resulting from a superposition of the three aforementioned spike varieties: [1] plateau potential, [2] initial spikelet, and [3] bAPs (**Fig. 1D$_2$**, **1D$_3$**, blue traces). To determine direction of propagation, we examined dendritic and somatic records on a faster time scale (**Fig. 1D$_{4\text{-}5}$**).

Initial Na^+ spikelet. The first peak in the dendritic voltage waveform was not a bAP, but rather a dendritic fast sodium spikelet at the beginning of the plateau that propagated orthodromically from dendrite to cell body. Initial spikelets ('init. s.') invariably failed to trigger a somatic or axonal AP, but ware clearly seen in somatic recordings (**Fig. 1D$_{4\text{-}5}$**, black traces). The peak of the dendritic sodium spikelet (blue arrow) occurred prior to its appearance in the soma (green vertical line). This spikelet has been previously shown to disappear in the presence of the sodium channel blocker, TTX[19,40].

Backpropagating action potentials (bAPs). Simultaneous dendritic and somatic recordings showed that plateau-triggered APs occurred in the cell body before the dendrite, thus indicating that somatic APs propagated from soma into the dendrites, riding atop the plateau potential (**Fig. 1D$_{4\text{-}5}$**). We found that bAPs could partially invade distal dendritic segments of basal dendrites even during local plateau depolarizations (**Fig. 1D$_1$**, ROIs; **Fig. 1D$_{2\text{-}3}$**, blue and red traces). bAP voltages were diminished in amplitude at the distal site (ROI-2) compared to the proximal site (ROI-1), clearly demonstrating the retrograde direction of propagation, from soma to dendrite. It is important to emphasize that the initial spikelet (**Fig. 1D$_3$**, "*init. s*") showed a completely opposite trend: initial spikelet voltages were diminished in amplitude at the cell body compared to the dendrite site (ROI-1) due to their orthograde direction of propagation, from dendrite to soma. Fast sodium spikelets propagating from dendrite to soma encounter a strong current sink imposed by the large amount of leaky membrane contained in the cell body and basal dendrites. The dendrite-originating initial spikelets fail to charge the cell body rapidly or sufficiently, thus failing to invade the soma[41,42].

II Simulation: computer model constrained by experimental measures

We built a full neuron model (**Fig. 2A$_{1-2}$**) with basal dendrites tuned to reproduce previously published data. These simulations matched experimental studies of bAPs (without plateaus) obtained previously[28,31], showing a ~18 mV/100 µm AP peak amplitude decrease with distance; AP backpropagation velocity: ~180 µm/ms (**Fig. 2B$_{1-3}$)**. Elimination of voltage-gated Na^+ channels (TTX condition) increased attenuation and decreased delay, while removal of A-type K^+ channels (4-AP condition) had opposite effects, matching bAP amplitude decrement with TTX or 4-AP measured experimentally[31].

Plateau potential activation is thought to be the result of synaptic activation on spine heads, as well as glutamate-spillover activation of extrasynaptic NMDARs on spine heads and necks, and on dendritic shafts (**Fig. 2C$_1$**)[43-46]. We did not explicitly model diffusion of glutamate but instead provided a delay of 5 ms to activate these receptors at the same location on the model dendrites (**Fig. 2C$_1$** bottom). A plateau potential could be obtained with just synaptic NMDAR activation (**Fig. 2C$_2$**, Control, green trace), but showed increased initial slope, amplitude, duration, and number of APs with the addition of extrasynaptic NMDAR activation (**Fig. 2C$_2$**, Control, black trace**)**. Plateau potential generation was dependent on adequate NMDAR activation and could be replicated in any oblique or basilar dendrite in both full morphology or in simplified neurons with one or more basilar/oblique dendrites. It was therefore robust to other changes in local ion channel densities, such as the elimination of Na^+ channels (**Fig. 2C$_2$**, TTX). It was also robust to moderate changes in NMDA parameters, including activation and inactivation time constants, and glutamate activation duration, and to glutamate stimulation location (see below). Simulations reproduced major behaviors seen experimentally in the present study (**Fig. 1**) including: (i) an inflection point on the rising phase at glutamate threshold (**Fig. 2D$_1$**, red arrowheads); (ii) plateau phase duration of 200-500 ms; (iii) the initial spikelet; (iv) bAPs and (v) abrupt plateau collapse (**Fig. 2D$_1$**).

Approximately 13% of basal dendrites are endowed with an ability to generate local sodium spikelets[40]; most likely due to higher local concentrations of Na^+ channels. Increasing the maximum sodium channel conductance (gNa_max) in basal dendrites by 25% had only minor effect on the plateau morphology (**Fig. 2D$_2$**). Next, we considered the temporal organization of incoming glutamatergic inputs impinging on the dendrite: comparing uniform random temporal distribution of synaptic activation (**Fig. 2E$_1$**) with grouping at the beginning of temporal window (**Fig. 2E$_2$**, “alpha”). The alpha-pattern grouping of the excitatory inputs slightly improved the

resemblance between model (**Fig. 2E$_3$**) and experimental measurement (**Fig. 2D$_3$**), producing a more abrupt initial rise 'r' (red arrows in **Fig. 2D$_{1\text{-}3}$)**.

Increased plateau duration with increased stimulation. In the next series of experiments, voltage-sensitive dye was replaced by Alexa Fluor 594 and recordings obtained in the cell body only. Increasing the intensity of the dendritic glutamatergic input (5 ms glutamate ejection on basal dendrites; 70–110 µm from soma center; n=15) in equal increments produced characteristic families of traces (**Fig. 3A**), which could be reproduced by simulation (**Fig. 3B**). In real neurons, the plateau amplitude at cell body showed a sigmoidal relation to the intensity of glutamatergic input presented on the dendrite (**Fig. 3C$_1$**, green). Similar distribution of the somatic plateau amplitudes was produced by our model (**Fig. 3C$_1$**, red). Despite the plateau amplitude saturation (**Fig. 3C$_1$**), cortical pyramidal neurons can interpret additional increases in glutamate input intensity by the means of plateau duration and AP firing. In both experiment and model, plateau duration increased monotonically with increasing glutamate stimulation (**Fig. 3C$_2$**), which in turn caused an increase in AP count (**Fig. 3C$_3$**).

We built two models based on two existing mechanisms for NMDAR conductances. Our “Model 1” employed the Destexhe *et al.*, 1994 NMDAR model, which mimicked our electrophysiological recordings with Type 1 morphology of the plateau collapse – gradual fall-off (**Suppl. Fig. S1A$_2$**). Our “Model 2” employed a more complex triple-exponential conductance model by Major *et al.*, 2008, and was able to match Type 2 morphology of the plateau collapse – abrupt drop (**Suppl. Fig. S1B$_2$**). Both Model 1 and Model 2 matched experimental plateau potential amplitudes, durations, and AP firing, all of which were similar for both Type 1 and Type 2 (**Suppl. Fig. S1CD**). Performance of the two models was also similar, except for a difference in glutamate threshold. The Major *et al* NMDAR model (Model 2) required stronger synaptic activation for the NMDA current to become regenerative (e.g. spike).

Although voltage-sensitive dyes report membrane potential changes with microsecond precision, with an optical signal directly proportional to membrane voltage, they cannot give precise voltage values for the dendritic plateau (in millivolts), because dendritic optical signals cannot be calibrated using the somatic patch electrode; explained in[28]. Therefore, we used the simulation results to estimate plateau amplitudes at the site or their origin, in distal segments of thin dendritic branches. Modeling exercises predict that the plateau phase of the dendritic plateau

potential is on average 57.6 ± 5.5 mV above resting membrane potential, or in the absolute range: -21 to -10 mV (24 stimulus locations 70–180 µm from soma center; 8 basal dendrites; both NMDAR models).

Somatic plateau durations were strongly correlated to dendritic plateau durations, both experimentally and in simulation (**Fig 4AB**; R^2=0.997 for simulation; 0.983 for experiment). While plateau durations (half-widths) were identical at all dendritic segments, the peak plateau amplitudes varied along the stimulated dendrite, being highest at the glutamate input site (**Fig. 4C**; input site at 85–115 µm). Plateau amplitude attenuated with distance from the input site with greater attenuation towards the soma and lesser attenuation towards the sealed end of the dendrite (**Fig. 4D**). bAP amplitudes (measured from plateau to peak, **Fig. 4C**, inset), on the other hand, were highest near the soma and attenuated to less than 5 mV at distal dendritic segments experiencing plateau potential (**Fig. 4E**, >100 µm). The attenuation of the bAP amplitudes was intensified around the glutamate input site (**Fig. 4E**, gray rectangle) suggesting a shunting effect imposed by the glutamate-activated dendritic conductances.

III The effect of input location on somatic depolarization amplitude

In published electrophysiological experiments (**Fig. 5A**), larger somatic plateau amplitude was associated with dendritic stimulation closer to the soma[6]. This experiment was reproduced in our model neuron (**Fig. 5B**), and showed distance fall-off similar to Major *et al* data (compare **Fig. 5A** and **Fig. 5C**). Inverting the axes for the averages of the model data (**Fig. 5C**) allowed us to estimate the distance from the dendritic initiation site (in µm) as a function of somatic plateau amplitude (amp in mV): [**Eqn. 1] Distance = 326 $e^{-0.073*amp}$ + 16** (Model 1); [**Eqn. 2] Distance = 323 $e^{-0.089*amp}$ + 40** (Model 2). For example, the somatic plateau amplitude of ~25 mV (**Fig 3A**) would indicate that glutamatergic activation was received ~68 µm away from the cell body, while amplitude 14 mV (**Suppl. Fig. S1B$_1$**) would indicate a ~128 µm distance. Overall estimated distance for the 15 cells studied ranged from 69 to 147 µm (average: 103 ± 19 µm).

Glutamate activation location only slightly affected amplitude at the stimulation location (**Fig. 5D**). This relatively subtle effect is explained by noting that plateau depolarizations are near the reversal potential of NMDAR voltage sensitivity, a ceiling effect. Location did have a substantial effect on plateau duration, an effect that could be seen in the soma as well as at the stimulus location (**Fig. 5BE**). Duration effects can be explained by the gradual increase in input

impedance (R_{in}) from proximal to distal, seen due to the sealed end of the dendrite (R_{in} in **Fig. 5E**).

Dendritic plateaus, propagating from dendrite to soma, often reach the threshold for AP initiation (**Fig. 3B**). The number of somatic APs depended on the glutamate input's distance from the cell body (**Fig. 5F**). In each model dendrite, we found a similar distance, 128 ± 12 µm (n=6 dendrites; both models), beyond which distal inputs were subthreshold for somatic AP generation (**Fig. 5F**, distal pool). Presence or absence of APs atop the plateau phase is another way for estimating the distance of the strong glutamatergic input onto a basal dendrite. Inputs more distal than ~130 µm typically produce spikeless plateau depolarizations in the cell body (**Fig. 5F**, distal pool). Although distal plateaus failed to drive AP initiation on their own, they caused sustained depolarizations of the cell body in the range of 10 to 20 mV. In the next series of experiments, we asked whether dendritic plateau potentials change the dynamics of the membrane response in the cell body.

IV Dendritic plateau potentials change global electrical properties of the neuron

To test the impact of dendritic plateau potentials on the overall neuronal membrane properties, input impedance (R_{in}) and membrane time constant (TAU), rectangular current pulses (test pulses) were injected into the cell body of a model neuron, while glutamatergic input was delivered in the mid segment of one basal dendrite (**Fig. 6A$_1$**, glut.). Simulations were performed in models with sodium channel blockade, mimicking treatment with TTX. Two test pulses of identical characteristics were delivered, before and during a glutamate-mediated plateau potential (**Fig. 6A$_1$**). The cell body response to a rectangular current pulse underwent drastic changes in both amplitude (**Fig. 6A$_2$**) and dynamics (**Fig. 6A$_3$**). A decrease in steady state amplitude (ΔVm) suggested that during a dendritic plateau potential, the cell body of the neuron was in a state of a lower Rin. Furthermore, the neuronal membrane response was faster (**Fig. 6A$_3$**, compare TAU-d vs. TAU-b). During a plateau, it took less time for the test-pulse-evoked voltage transient to reach 63% of its maximal amplitude (**Fig. 6A$_3$**, 63%), that is, during dendritic plateau potential the somatic TAU (TAU-d) is markedly shorter than the TAU measured before plateau onset (TAU-b).

In simulation, a current-evoked steady-state depolarization during plateau (ΔVm-d) was on average 48 ± 1.5 % of the ΔVm value measured before plateau, ΔVm-b (**Fig. 6D$_1$**, Model Neuron) (mean ± stdev; n = 16 trials, 16 dendrites stimulated, in two model cells). Membrane time constant during plateau (TAU-d) was on average 40.8 ± 2.2 % of the TAU value measured before plateau, TAU-b (**Fig. 6D$_2$**, Model Neuron). Using sinusoidal current injections into the cell body we found that neuronal impedance decreases during plateau potential (**Suppl. Fig. S3**). The effect was strongest at low frequencies (5 and 10 Hz), and negligible at stimulus frequencies greater than 75 Hz (**Suppl. Figs. S4 - S7**).

These model predictions were tested by subsequent experiments in brain slices. The experimental paradigm in brain slices (**Fig. 6B$_1$**) was identical to the one used in simulation (**Fig. 6A$_1$**). Both positive (**Fig. 6B$_2$**, i) and negative test pulses (**Fig. 6B$_2$**, ii) were used to assess somatic membrane response in TTX-treated layer 5 pyramidal neurons. Additional recordings were made with test pulses omitted, i.e. glutamatergic stimulation only (**Fig. 6B$_2$**, iii). The contour of glutamate-induced plateau, unaltered by test pulses, is useful for offline subtraction of traces. For example, the trace shown in **Fig. 6C$_1$** is arithmetic subtraction of trace “iii” from trace “i” (raw traces “i” and “iii” are shown in **Fig. 6B$_2$**). This subtraction procedure eliminated undulations in the baseline caused by underlying plateau.

In experiments with positive test pulses, test pulse-induced somatic voltage transients were smaller in amplitude (ΔVm) and faster to rise (shorter TAU), compared to the same test performed on the same neuron just before the plateau onset (**Fig. 6C$_3$**). Quantification of the electrophysiology data showed that, in cortical layer 5 pyramidal neurons, a current-evoked depolarization during plateau (ΔVm) was on average 63.1 ± 5.1 % of the ΔVm value measured before plateau (**Fig. 6D$_1$**, Real Neuron). Membrane time constant (TAU) during plateau was on average 70.3 ± 5.1 % of the TAU value measured just before plateau (**Fig. 6D$_2$**, Real Neuron; n=30 recordings (trials) obtained by stimulating 17 dendrites in 13 pyramidal neurons). In summary, when a positive test pulse is used for estimating somatic membrane response, the percent fall-off in ΔVm (**Fig. 6D$_1$**) and TAU (**Fig. 6D$_2$**) was comparable between simulation and experiment (Model Neuron vs. Real Neuron). When positive test pulses were used in real neurons, plateau-induced changes matched the direction of those predicted by the model (**Fig. 6D$_{1\text{-}2}$**, arrows pointing downwards). However, in several experimental trials (n = 4 out of 30) we found TAU-d to be similar or even greater than TAU-b. The baseline voltage of the plateau

phase is unstable and difficult to control in experiments (**Fig. 6BC**), so distortions in the charging curve may have contributed to large TAU values occasionally. With these outliers included in the current data set, the precise magnitudes of the plateau-induced reductions of the soma TAU were different between model and real neurons. Both model neurons and real neurons showed plateau-induced shortening of TAU (**Fig. 6D$_2$**, downward arrows), but the degree of shortening was significantly greater in model; p = 0.014, unpaired T-test.

Next, we used negative test pulses to assess neuronal membrane properties before and during glutamate-evoked dendritic plateau potential. With negative polarity of test pulse, the “before” and “during” voltage waveforms were of similar amplitude (ΔVm) and similar dynamics (TAU) (**Fig. 6C$_4$**). Negative pulse group comprised n=18 traces obtained by stimulation of 11 basal dendrites in 7 pyramidal cells. We found a discrepancy between data obtained with positive versus negative test pulses. More specifically, in real neurons explored with positive test pulses, a current-evoked depolarization during plateau (ΔVm) was on average 63.1 ± 5.1 % of the ΔVm value measured before plateau (**Fig. 6E$_1$**, Positive test pulse, 30 recordings obtained by stimulating 17 dendrites in 13 pyramidal neurons). When negative test pulses were used in cortical layer 5 pyramidal neurons, ΔVm did not change notably 100.4 ± 7.4 % (**Fig. 6E$_1$**, Negative test pulse, 18 recordings obtained by stimulation of 11 basal dendrites in 7 cells) and membrane TAU during plateau became longer than before the plateau, 131.4 ± 9.5 % (**Fig. 6E$_2$**, *Negative test pulse*). For both parameters of the membrane response, ΔVm and TAU, the differences between the sets of values obtained with positive vs. negative pulses were highly significant (p<0.0001) (**Fig. 6E$_{1\text{-}2}$**, asterisks).

We have shown that glutamatergic inputs arriving in proximal segments of basal dendrites, closer to the cell body, produce greater somatic depolarizations than input received in distal dendritic segments, far away from the cell body (**Fig. 5**). Next, we asked whether proximal dendritic inputs exert stronger influence on the dynamics of the somatic membrane response. By gradually changing the location of glutamatergic input along model basal dendrites and measuring soma TAU on each trial (**Fig. 7A$_{1\text{-}2}$**), we found that plateau-induced shortening of the soma TAU strongly depends on the distance between the cell body and glutamate input site. With identical (fixed) intensity, proximal inputs exerted more prominent shortening of the soma TAU than distal inputs (**Fig. 7B$_{1\text{-}2}$**).

V Plateau potentials affect synaptic integration

The plateaus provided a depolarized potential that brought the membrane closer to firing threshold. This was expected to enhance the effects of excitatory postsynaptic potential (EPSP) inputs on spiking. Additionally, the decrease in TAU for depolarizing current stimuli, will allow faster membrane charging to also enhance EPSP efficacy in producing a spike. However, the reduction in R_{in} will reduce EPSP amplitude and reduce efficacy. To assess these countervailing influences, we simulated a spatially-distributed EPSP barrage (**Fig. 8A$_1$**) before and during the plateau. The EPSP barrage, subthreshold before the plateau (**Fig. 8A$_2$**, EPSPs before plateau), caused AP firing when it arrived during the plateau (**Fig. 8A$_2$**, "EPSP-evoked AP"). An AP due to the EPSP barrage could also be detected in the context of additional somatic APs associated with the plateau itself (**Fig. 8B$_{1\text{-}2}$**). The timing of the intercalated EPSP-associated spike was closely tied to EPSP time (**Fig. 8B$_{1\text{-}2}$**, "EPSP-evoked AP"). This is to say that both "spikeless plateaus" (**Fig. 8A**) and "spiking plateaus" (**Fig. 8B**) increase the capacity of cortical neurons to respond to afferent EPSPs by generation of new APs.

Next, a temporal delay (dT) from EPSP to AP was used as a measure of the neuronal responsiveness to incoming afferent inputs. In simulation, the dendritic plateau potential was kept at a fixed time delay from the beginning of the experimental trace (time point 200 ms). That is, the onset of the glutamate-evoked plateau was always at 200 ms in respect to the beginning of the trial (0 ms). In repeated trials, we systematically changed the timing of the EPSP barrage (from 0 to 600 ms), while keeping the plateau at 200 ms. The EPSP-to-AP temporal delay (dT) was reduced from ~13 ms before plateau to ~6 ms during plateau (**Fig. 8C$_1$**). This time interval between EPSP and AP (dT) precisely followed the contours of the plateau voltage waveform (**Fig. 8C$_2$**), suggesting causality.

Discussion

We used optical imaging to characterize voltage waveforms of glutamate-mediated plateau potentials occurring in basal and oblique dendrites of neocortical layer 5 pyramidal neurons. By employing a gradually increasing intensity of the focal glutamatergic input, we documented the transitions between subthreshold to threshold regenerative local potentials, occurring at the dendritic site of initiation. These sets of voltage waveforms, obtained at different levels of excitatory input, and simultaneously recorded at dendrite and soma, provided constraints for simulation of a cortical pyramidal neuron. The modeling data obtained with the detailed model (realistic morphology + uneven spatial distributions of membrane conductances) demonstrated that dendritic plateau potentials changed the state of pyramidal cells in a profound way, with implications for neuronal network information processing. During dendritic plateau potentials, cell bodies of pyramidal neurons are placed in a depolarized state closer to the AP firing threshold. During this sustained depolarized state, the somatic membrane shows a notably faster capacitative charging in response to depolarizing currents (i.e. excitation). As a result of dendritic plateaus, pyramidal neurons are more responsive to afferent synaptic activity arriving anywhere on the complex dendritic tree. Barrages of EPSPs, which are subthreshold before the plateau, become more successful drivers of axo-somatic APs during the plateau. In addition, dendritic plateaus accelerate initiation of the EPSP-induced APs. The time delay between the onset of EPSPs and the onset of EPSP-induced AP (dT) is notably shorter during the plateau. Faster EPSP-to-AP transition rates are expected to improve neuronal ability for “tuning” into fast rhythmic afferent synaptic and network activities. Dendritic plateau potentials move cortical pyramidal neurons from resting state (‘Down state like’) into a more excitable state (‘Up state like’); a sustained depolarized state during which afferent inputs are more effective and the transformation of afferent excitatory inputs into postsynaptic AP firing is much faster.

Dendritic voltage waveforms.

Over the years, researchers have used somatic recordings to study initiation of local spikes in basal and oblique dendrites of pyramidal neurons. Within somatic recordings, they searched for “kinks” which may represent filtered and decremented versions of the original dendritic spike waveforms[47,48]. A lot has been learned about the behavior and ionic composition of local dendritic spikes without ever showing what dendritic spikes look like at the thin dendrite[47,48]. In the current study, we overcame the limitations of the earlier explorations by employing an

optical imaging method capable of tracking membrane potential changes at microsecond resolution[49]. We show that glutamate-mediated local dendritic spikes are complex waveforms comprised of several phases including a rapid rise, initial spikelet, plateau segment and abrupt collapse back to resting membrane potential (**Fig. 1C**).

In one prior study, researchers were able to patch basal dendrites with micropipettes of very high electrical resistance, resulting in dendritic whole-cell recordings of high series resistance[19]. They found that synaptic stimulations generate rectangular local dendritic potentials, while direct current injections generated local sodium spikes in some basal dendrites. Our current study explored several aspects of dendritic potentials which were not measurable in the prior study. First, we explored how gradual increase in glutamatergic input triggers local regenerative potentials in dendrite. The previous study did not explore dendritic voltage in response to gradually increasing input. Second, we showed that sodium spikelets were initiated by glutamatergic inputs. The previous study used direct current injection to activate sodium channels. Third, we showed that sodium spikelets precede the plateau phase and are responsible for the same kinks in the somatic recordings previously correctly interpreted as dendritic spikes in basal and oblique branches[47,48]. Fourth, we made recordings from two dendritic sites simultaneously (**Fig. 1D**) allowing for a better understanding of dendritic voltage maps. The previous study was restricted to one recording site per dendrite. Fifth, we described propagation of glutamate-evoked sodium spikelets and plateau potentials from dendrite to soma and simultaneous propagation of APs traveling from soma to dendrite. These three types of potentials met in the mid segments of dendritic branches resulting in complex waveforms, which have not be identified previously by patch electrode recordings in basal dendrites[19].

Experimental constraints on the current model. Our model of plateaus and back-propagating action potentials (bAPs) in a cortical pyramidal neuron was constrained by 4 sets of experimental data: (i) voltage waveforms obtained at the site of the glutamatergic input in distal basal dendrite, including initial sodium spikelet, fast rise, plateau phase and abrupt collapse of the plateau; (ii) a family of voltage traces describing dendritic membrane responses to gradually increasing intensity of glutamatergic stimulation (**Fig. 1AB**, ‘dend’); (iii) voltage waveforms of backpropagating action potentials in basal dendrites[28]; and (iv) the change of bAP amplitude in response to drugs that block Na^+ or K^+ channels[31].

Extrasynaptic NMDAR channels. Glutamatergic synapses are functionally clustered on dendrites; the neighboring synapses in one dendrite activate together more often than the synapses scattered on many branches[1,50,51]. Repetitive clustered synaptic stimulation has been shown to overcome the ability of astrocytic processes to clear glutamate[7,45], and can actually induce astrocytic glutamate release through reversal of astrocyte glutamate transporters[52]. This would allow excitatory neurotransmitter to spill-over from synaptic clefts to activate extrasynaptic NMDA receptors between dendritic spines[53-57]. Glutamate diffusion from synaptic clefts to extrasynaptic NMDA receptors has been shown with two-photon calcium imaging during synaptically-evoked NMDA spikes (2 synaptic stimuli at 50 Hz) on both spines and dendritic shafts[45].

Direct immunostaining has found a similar density of NMDARs at synaptic and extrasynaptic locations[58]. A kinetic study showed no major differences in dynamics between NMDARs at these two locations[59]. This led us to set magnitudes of synaptic and extrasynaptic NMDA conductances at a 1:1 ratio, and to use the same membrane mechanism for both (Methods). We implemented a 5 ms time delay to account for time required for glutamate diffusion from synaptic cleft to dendritic shaft.

Our model demonstrated dendritic plateaus even without glutamate spillover. However, adding the activation of extrasynaptic NMDARs improved three cardinal features of dendritic plateau potentials (**Fig. 2C$_2$**). Namely, activation of extrasynaptic NMDARs produces: [a] faster rising, [b] longer lasting, and [c] larger amplitude somatic plateau depolarizations. We speculate that the major difference between typical dendritic NMDA spikes, which last ~50 ms[39], and typical dendritic plateau potentials, which last 200 – 500 ms[4,7], may lie in the extent to which a released glutamate is maintained around dendrite (due to a standstill in the astrocytic uptake)[46] causing the activation of extrasynaptic NMDARs.

Model predictions:

1. **Plateau initiation location can be predicted from somatic plateau amplitude** (**Fig. 4D**). Equations [1] & [2] permit us to estimate the likely distance of plateau origin based on the waveform measured in the soma. This prediction could be tested by direct measurement with precision glutamate uncaging[47].

2. **Plateau durations are greater when triggered from more distal dendritic segments** (**Fig. 5E**, “duration”). This effect is due to higher distal local effective R_{in} (**Fig. 5E**, “R_{in}”).

The waveform of the NMDA current interacts with the local R_{in} to generate a local voltage transient ($\Delta Vm = R_{in} * I_{NMDA}$). In distal dendritic segments equipped with higher R_{in} the same current waveform, as it decays in time, produces greater voltage deflections (for longer time) thus giving local plateau potentials longer durations. Although technically difficult, this prediction could be tested by applying glutamatergic inputs of fixed intensity at several sites along the same basal dendrite[4,6]. If confirmed in real neurons, this finding would have important implications on the development-meditated or experience-mediated positioning of synaptic clusters[50] along dendrites. Distally positioned functional synaptic clusters would produce longer sustained depolarizations, with potential impacts on cortical processing of information[27].

3. **Proximal and distal dendritic zones have different AP-generation properties.** As glutamate input location is moved away from the soma, somatic plateau depolarization amplitude decreases rapidly[4,6]. This "distance-dependence" segregates roughly the basal dendrite into proximal and distal region -- only proximal dendritic segments will generate APs on the somatic plateau (**Fig. 5F)**. We predict that this this distal "no-AP-generation region" begins at 110-130 µm in most basal dendrites (**Fig. 5F)**. Further measurements would be able to determine if these two functionally-defined dendrite sections (proximal or distal) also have other zone specializations, such as density of NMDARs, density of Ca^{2+} channels, additional spine specialization, or selection of afferent inputs originating from distinct brain regions or carrying the same type of information (e.g. 'proximal or distal drivers' discussed in ref. [22]).

4. **Proximal and distal dendritic zones for bAPs.** Distance-dependence is also seen in the centrifugal direction: bAPs from soma to dendrite are readily seen above the plateau at proximal, but not at distal locations (**Fig. 4C**). When a plateau is initiated at ~100 µm, the bAP riding atop the plateau declines in amplitude abruptly at about 80-100 µm (**Fig. 4E)**. By contrast, when a plateau is absent, the bAP maintains significant amplitude up to ~150 µm (**Fig. 2B$_2$**, black line). Long lasting dendritic plateau potentials are less affected by cable RC filtering than brief sodium APs. Compared to the forward propagation of long-lasting plateaus (from dendrite to soma), backpropagation of brief APs on top of plateau (from soma to dendrite) is more limited due to several additional factors: (i) lack of regenerative Na^+ channel activation due to low channel density in dendrite; (ii) plateau-induced depolarization-related Na^+ channel partial inactivation; (iii) shunting

through AP-activated A-Type K^+ channels[19,31]; (iv) shunting through the large NMDAR conductance at the glutamate input site (**Fig. 4C**).

5. **Plateau-evoked bAPs will interact with the plateau in the dendrite of origin, producing more Ca^{2+} influx.** Glutamate-mediated dendritic plateau potentials cause a substantial influx of Ca^{2+} along the entire branch[60-62]. Our dendritic recordings, as well as modeling data, show a partial invasion of bAP traveling atop plateau potentials; invasion limited to proximal dendritic segments (**Fig. 4CE**). These data suggest that distinct AP-associated Ca^{2+} transients would ride on top of a NMDA-dependent Ca^{2+} influx during glutamate-mediated dendritic plateau potential, to drive spike timing dependent plasticity (STDP)[63] in the proximal, but not in the distal region of basal dendrites.

6. **Membrane time constant is shortened during a plateau.** This prediction of the model was tested and confirmed in real neurons (**Fig. 6**). Depolarizations (induced by positive transmembrane currents) occurring during plateau potential seem to be affected by a glutamate-induced decrease in R_{in} (to a larger extent), and also by the test-pulse-induced partial activation of voltage gated conductances (to a smaller extent). These two factors force the neuronal charging curve to reach its steady state sooner compared to before plateau (shorter TAU).

   However, hyperpolarizing currents (i.e. negative test pulse) injected into the cell body during the plateau phase did not produce shorter TAUs in our measurements (**Fig. 6C_4**). This was probably due to antagonistic voltage interactions between negative test pulse and voltage gated conductances (e.g. NMDA, VGCC, h-current). Basically, negative pulses tend to close the neuronal voltage gated channels. The larger negative vs positive pulse response on the plateau is indicative of a strong fast transient increase in conductance for positive pulses and a strong decrease in conductance for negative. Another contributing factor may be the undulating baseline voltage during the plateau, distorting the exponential fits.

7. **Synaptic responses are more effective during plateau potential.** The most obvious factor increasing spike probability (in response to EPSPs) is the depolarization itself, which shifts the somatic (and axon initial segment) potential approximately 20 mV closer to spike threshold (**Fig. 3C_1**). An additional factor increasing spike probability is the increased speed of response due to decreased membrane time constant in the cell body (**Fig. 6**). EPSPs with faster rise times are more powerful activators of the voltage-gated

sodium current due to the channel activation kinetics being faster than inactivation kinetics[64-66].

Limitations of the model. Our model is currently a special purpose model with a focus on the phenomenology of dendritic plateaus in the context of basilar and oblique dendrites. The model also has been tuned to accurately match these, and to also match prior data on back-propagating APs (bAPs) with and without channel blockers. Further extension and tuning of the model will be needed to also reflect bAPs, and synaptic integration at the apical nexus and tufts above[49]. Additional improvements will allow us to combine this model with our prior models of corticospinal (thick-tufted) and corticostriatal (thin-tufted) Layer 5 pyramidal cells[67,68].

Figure legends

Figure 1. Voltage waveforms of dendritic plateau potentials.
(A_1) Pyramidal neuron filled with JPW-3028. Area inside rectangle is imaged at 2.7 kHz, but only one dendrite is illuminated by laser spot. **(A_2)** The intensity of the glutamatergic stimulation was increased in equal steps through 9 recording trials (Trials 1-9), while optical signals were recorded in the dendritic region of interest (ROI). "Soma" marks the somatic whole cell recordings. (**B**) Same experimental paradigm as in *A,* except different cell. (**C**) Glutamatergic stimulation of an oblique dendrite (duration 5 ms) triggers a local plateau potential. r-fast rise; s-initial sodium spikelet; p-plateau phase; c-collapse of the plateau. (**D_1**) Same experimental paradigm as in *A,* except different cell. (**D_2**) In Trial 1, glutamate-induced membrane potential changes are recorded simultaneously at two ROIs on the same dendrite and in the cell body (whole-cell). (**D_3**) In Trial 2, the glutamatergic stimulus was increased by 20% causing a longer lasting plateau phase. The initial spikelet in the somatic recordings (black arrow) is caused by the initial spikelet in the dendritic recording (blue arrow). The rapid inflection preceding the plateau phase (red arrowhead) is also present in the somatic whole-cell recordings (red arrowhead). Three backpropagating APs (bAPs) recorded in dendrite are marked by black arrows. (**$D_{4,5}$**) Blowups of *D_2* and *D_3* on faster time scales to show that initial spikelet (init. s.) precedes the somatic kink.

Figure 2. Model outline.
(A_1) Reconstructed pyramidal neuron. **(A_2)** Six basal dendrites, mostly used in data quantifications, are labeled by bracketed numbers. **(B_1)** The bAP amplitude, peak latency, response to TTX and 4-AP match the experimental measurements obtained in basal dendrites using voltage sensitive dyes. (**$B_{2,3}$**) Quantification of the model results. **(C_1)** Glutamate stimulations activate the AMPA and NMDA receptors on dendritic spines (red) and the NMDA receptors on extrasynaptic surfaces (yellow), including the spine head, spine neck, and dendritic shaft. **(C_2) (upper)** Green = Somatic response evoked by synaptic NMDARs only. Black - Somatic response evoked by conjugate activation of both synaptic and extrasynaptic NMDARs. **(lower)** Same traces as in *C_2-upper*, but with the application of TTX to block all voltage-sensitive sodium channels. **(D_1)** Membrane potential change in basal dendrite during a plateau potential. **(D_2)** Same as in *D_1*, except gNa_bar increased by 25%. **(D_3)** Membrane potential change in basal dendrite obtained by voltage-sensitive dye imaging (*from Fig.1D_3*). **(E_1)** Temporal organization of the glutamatergic inputs – uniform random within time window of 65 ms. Presynaptic axons (green) impinging on dendritic spines (brown). Ticks indicate APs in axon. **(E_2)** Temporal organization of inputs – alpha random function. **(E_3)** Dendritic plateau potential with alpha distribution of inputs. "r", "s", "p", & "c" same definition as in Fig. 1.

Figure 3. Varying levels of glutamatergic input in experiments and model.
(A) Somatic whole cell recordings in a layer 5 pyramidal neuron. Glutamate microiontophoresis was applied on one basal branch ~90 µm away from the soma. The intensity of the glutamate iontophoretic current was increased gradually in equal steps. **(B)** Computational model of the simultaneous somatic and dendritic voltage response to glutamate application on one basal dendrite. Distance from the soma = 110 µm. The NMDAr mechanism here is based on Destexe et al., 1994 (our Model 1). The Model 2 data (employing the Major et al., 2008 NMDAr mechanism) is shown in *Suppl. Fig. S1B*. **(C_{1-3})** Quantification of the experimental data obtained in 3 real neurons (green) and 2 model neurons (red).

Figure 4. Voltage waveforms in soma and dendrite are strongly correlated.
(A) Comparisons between dendritic and somatic voltage transients obtained in the model simulations. n = 70 sweeps in 6 model basal branches. Insets depict the method used for measuring plateau amplitude and duration (half-width) in dendrite and soma. **(B)** Experimental measurements in rat brain slices using simultaneous recordings of voltage waveforms in dendrite (voltage imaging) and soma (whole-cell). n = 19 sweeps from 5 pyramidal neurons. Linear fitting by ordinary least squares regression. The 95% confidence interval is marked by gray shading. **(C)** Computer simulation. Dendritic voltage waveforms obtained simultaneously from 13 locations along basal dendrite and cell body (soma). Inset: bAPs emerge from the plateau phase. Lower horizontal lines "plat." mark the amplitude of the plateau phase. Two-sided arrow indicates method used for measuring "*AP amplitude above plateau*". **(D)** Dendritic plateau amplitude ("plat.") as function of distance from cell body. **(E)** Amplitude of bAPs above plateau level, as function of distance from cell body.

Figure *5.* Plateau properties depend on the input location along dendrite.
(A) Glutamate microiontophoresis was delivered on the basal branches at various distances from the cell body and membrane potential changes recorded in the soma. The amplitude of the plateau potential in the soma is plotted against the distance from the cell body – recreated from Major et al., 2008. **(B)** Computer simulation of the experiment described in *A*. Results obtained with our "Model 2" (employing Major et al., 2008 NMDAr mechanism) are displayed – simultaneous voltage waveforms in dendrite (at input location) and soma. The precise locations of the glutamate inputs on basal dendrite are annotated above each dendritic trace and expressed as a distance from the cell body in micrometers. Vertical dashed lines mark 4 different plateau durations obtained by stimulating basal dendrite at 4 locations – fixed glutamate input intensity. The results of Model 1 (utilizing the Destexe et al. (1994) membrane mechanism for NMDAr channels) are shown in *Suppl. Fig. S2B*. **(C)** Same as *A*, except model neuron data quantification. **(D)** The local amplitude of the dendritic plateau, measured at each glutamate stimulation site, is plotted versus the distance of that stimulation site from the cell body. **(E)** The local duration (half-width) of the dendritic plateau at the glutamate stimulation site is plotted as a function of distance from the cell body. Blue data points depict local dendritic R_{in}. **(F)** Distal glutamatergic inputs (distal pool) generate dendritic plateau potentials, which fail to trigger somatic APs.

Figure 6. Dendritic plateau potential affects the cell body Rin and TAU.
(A_1) Basilar dendritic tree of the model cell. Dendritic segment (66–132 µm) is receiving glutamate inputs. Computer simulation of dendritic plateau potential measured at soma. An identical depolarizing current pulse was injected into the soma before and during the plateau potential (current injection). **(A_2)** Same as in ***A_1***, except, before (black trace) and during (gray trace) are superimposed. (A_3) Same as in ***A_2*** except traces are amplitude scaled. **(B_1)** Experimental outline. Whole-cell recordings from cortical L5 pyramidal neuron treated by TTX. Glut. - glutamate pulse (5 ms) was delivered on one basal dendrite (90 µm away from the cell body). Rectangular current pulses (test pulses) were injected into the cell body at two time points, *Before* and *During* glutamate-evoked plateau potential. **(B_2)** Three experimental trials obtained in the same layer 5 pyramidal cell. Experimental paradigm consisted of pairing dendritic plateau potentials with test pulses injected into the cell body. Each trace is an average of 5-7 sweeps obtained from the same cell. **(C_1)** Arithmetic subtraction of traces "i" and "iii" (shown in ***B_2***). **(C_2)** Arithmetic subtraction of traces "ii" and "iii". **(C_{3-4})** Test-pulse-evoked somatic voltage transients are superimposed (same scales). **(D_1)** Relative changes in the amplitude of the test pulse-evoked transients (ΔVm) in model and real neurons. A value obtained during plateau was normalized by the value obtained before plateau onset in the same neuron. **(D_2)** Relative plateau-induced changes in TAU obtained in model and real neurons. A TAU value obtained during plateau was normalized by the TAU value obtained in the same neuron before plateau. **(E_1)** Measurements were obtained in real neurons in brain slices. Mean relative change in the amplitude of ΔVm, depending on the polarity of test pulse (positive vs. negative). **(E_2)** Mean relative change in TAU (induced by plateau), depending on the polarity of the test current. n = number of experimental trials (number of dendrites and number of cells are specified in text).

Figure 7. Position of glutamatergic input on basal dendrite determines the plateau-induced changes of soma TAU.
(A_1) In a model cell void of Na^+ channels (to mimic a TTX condition in brain slice experiments), glutamate input of fixed intensity was delivered at two different locations along a basal dendrite. **(A_2)** At a proximal location (red), the amplitude of the glutamate-mediated dendritic plateau potential observed from the cell body (red trace) is greater compared to the same experiment performed at distal dendritic location (green trace). A test pulse-evoked membrane charging curve is faster during proximal glutamatergic inputs (red trace). Vm-t marks the membrane voltage at which the test pulse begins. **(B_1)** Data shown in panel A_2 suggest dependence of soma TAU on the distance of glutamate input from the soma. To determine if this relation holds in basal dendrites of different morphologies, glutamate location was varied along each branch, while input intensity was kept unchanged. **(B_2)** Quantification of data for experiment shown in B_1. Note that every basal dendrite tested in this model (n=6) showed a similar relation between soma TAU versus the distance at which glutamate input was delivered. Overall, the soma membrane response becomes faster (shorter TAU) if glutamate input is closer to the cell body.

Figure 8. Plateau potential accelerates EPSP-to-AP transition.
(A_1) Basilar dendritic tree of the model cell. "Plateau" marks glutamatergic input site. **(A_2)** Blue trace: A barrage of EPSPs (individual EPSPs were received at 5 locations marked by blue arrows in *A_1*) was delivered on two distinct time points. Orange trace: Glutamatergic stimulation of one basal dendrite produced a somatic plateau subthreshold for axonal AP initiation (spikeless plateau). Black trace: pairing of the stimulation paradigms used in the blue and orange trace. **(B_1)** The same modeling experiment as in *A_2*, except the EPSP barrages were paired with a more proximal plateau potential, accompanied by two APs (spiking plateau). **(B_2)** The same modeling experiment as in *B_1*, except an even stronger plateau, with more accompanying APs, was used for pairing. **(C_1)**

Upper trace: Strong EPSP barrage, capable of triggering AP in the absence of plateau. Lower trace: Pairing of the strong EPSP barrage with a spikeless plateau. Vertical blue line: onset of EPSP barrage. Vertical red line: Peak of the EPSP-evoked AP. Green box: Time delay between the onset of EPSP barrage and the AP peak. **(C_2)** Onset of EPSP barrage was gradually shifted in time, while the onset of plateau potential was fixed in time. Time delay (dT) is plotted versus the absolute time of the experimental trial (sweep). Initiation of the plateau potential shortens the time delay, dT.

References

1. Kleindienst, T., J. Winnubst, C. Roth-Alpermann, T. Bonhoeffer, and C. Lohmann, *Activity-dependent clustering of functional synaptic inputs on developing hippocampal dendrites.* Neuron, 2011. **72**(6): p. 1012-24.

2. Makino, H. and R. Malinow, *Compartmentalized versus global synaptic plasticity on dendrites controlled by experience.* Neuron, 2011. **72**(6): p. 1001-11.

3. Lee, K.F., C. Soares, J.P. Thivierge, and J.C. Beique, *Correlated Synaptic Inputs Drive Dendritic Calcium Amplification and Cooperative Plasticity during Clustered Synapse Development.* Neuron, 2016. **89**(4): p. 784-99.

4. Milojkovic, B.A., M.S. Radojicic, P.S. Goldman-Rakic, and S.D. Antic, *Burst generation in rat pyramidal neurones by regenerative potentials elicited in a restricted part of the basilar dendritic tree.* J Physiol, 2004. **558**(Pt 1): p. 193-211.

5. Milojkovic, B.A., M.S. Radojicic, and S.D. Antic, *A strict correlation between dendritic and somatic plateau depolarizations in the rat prefrontal cortex pyramidal neurons.* J Neurosci, 2005. **25**(15): p. 3940-51.

6. Major, G., A. Polsky, W. Denk, J. Schiller, and D.W. Tank, *Spatiotemporally graded NMDA spike/plateau potentials in basal dendrites of neocortical pyramidal neurons.* J Neurophysiol, 2008. **99**(5): p. 2584-601.

7. Suzuki, T., S. Kodama, C. Hoshino, T. Izumi, and H. Miyakawa, *A plateau potential mediated by the activation of extrasynaptic NMDA receptors in rat hippocampal CA1 pyramidal neurons.* Eur J Neurosci, 2008. **28**(3): p. 521-34.

8. Takahashi, H. and J.C. Magee, *Pathway interactions and synaptic plasticity in the dendritic tuft regions of CA1 pyramidal neurons.* Neuron, 2009. **62**(1): p. 102-11.

9. Plotkin, J.L., M. Day, and D.J. Surmeier, *Synaptically driven state transitions in distal dendrites of striatal spiny neurons.* Nat Neurosci, 2011. **14**(7): p. 881-8.

10. Lavzin, M., S. Rapoport, A. Polsky, L. Garion, and J. Schiller, *Nonlinear dendritic processing determines angular tuning of barrel cortex neurons in vivo.* Nature, 2012. **490**(7420): p. 397-401.

11. Xu, N.L., M.T. Harnett, S.R. Williams, D. Huber, D.H. O'Connor, K. Svoboda, and J.C. Magee, *Nonlinear dendritic integration of sensory and motor input during an active sensing task.* Nature, 2012. **492**(7428): p. 247-51.

12. Smith, S.L., I.T. Smith, T. Branco, and M. Hausser, *Dendritic spikes enhance stimulus selectivity in cortical neurons in vivo.* Nature, 2013. **503**(7474): p. 115-20.

13. Gambino, F., S. Pages, V. Kehayas, D. Baptista, R. Tatti, A. Carleton, and A. Holtmaat, *Sensory-evoked LTP driven by dendritic plateau potentials in vivo.* Nature, 2014. **515**(7525): p. 116-9.

14. Cichon, J. and W.B. Gan, *Branch-specific dendritic Ca(2+) spikes cause persistent synaptic plasticity.* Nature, 2015. **520**(7546): p. 180-5.

15. Du, K., Y.W. Wu, R. Lindroos, Y. Liu, B. Rozsa, G. Katona, J.B. Ding, and J.H. Kotaleski, *Cell-type-specific inhibition of the dendritic plateau potential in striatal spiny projection neurons.* Proc Natl Acad Sci U S A, 2017. **114**(36): p. E7612-E7621.

16. Ranganathan, G.N., P.F. Apostolides, M.T. Harnett, N.L. Xu, S. Druckmann, and J.C. Magee, *Active dendritic integration and mixed neocortical network representations during an adaptive sensing behavior.* Nat Neurosci, 2018. **21**(11): p. 1583-1590.

17. Gordon, U., A. Polsky, and J. Schiller, *Plasticity compartments in basal dendrites of neocortical pyramidal neurons.* J Neurosci, 2006. **26**(49): p. 12717-26.

18. Evans, R.C., T. Morera-Herreras, Y. Cui, K. Du, T. Sheehan, J.H. Kotaleski, L. Venance, and K.T. Blackwell, *The effects of NMDA subunit composition on calcium influx and spike timing-dependent plasticity in striatal medium spiny neurons.* PLoS Comput Biol, 2012. **8**(4): p. e1002493.

19. Nevian, T., M.E. Larkum, A. Polsky, and J. Schiller, *Properties of basal dendrites of layer 5 pyramidal neurons: a direct patch-clamp recording study.* Nat Neurosci, 2007. **10**(2): p. 206-14.

20. Larkum, M.E., T. Nevian, M. Sandler, A. Polsky, and J. Schiller, *Synaptic integration in tuft dendrites of layer 5 pyramidal neurons: a new unifying principle.* Science, 2009. **325**(5941): p. 756-60.

21. Rhodes, P., *The properties and implications of NMDA spikes in neocortical pyramidal cells.* J Neurosci, 2006. **26**(25): p. 6704-15.

22. Jadi, M., B.F. Behabadi, A. Poleg-Polsky, J. Schiller, and B.W. Mel, *An augmented 2-layer model captures nonlinear analog spatial integration effects in pyramidal neuron dendrites.* Conf Proc IEEE Eng Med Biol Soc, 2014.

23. Bono, J. and C. Clopath, *Modeling somatic and dendritic spike mediated plasticity at the single neuron and network level.* Nat Commun, 2017. **8**(1): p. 706.

24. Doron, M., G. Chindemi, E. Muller, H. Markram, and I. Segev, *Timed Synaptic Inhibition Shapes NMDA Spikes, Influencing Local Dendritic Processing and Global I/O Properties of Cortical Neurons.* Cell Rep, 2017. **21**(6): p. 1550-1561.

25. Legenstein, R. and W. Maass, *Branch-specific plasticity enables self-organization of nonlinear computation in single neurons.* J Neurosci, 2011. **31**(30): p. 10787-802.

26. Chiovini, B., G.F. Turi, G. Katona, A. Kaszas, D. Palfi, P. Maak, G. Szalay, M.F. Szabo, G. Szabo, Z. Szadai, S. Kali, and B. Rozsa, *Dendritic spikes induce ripples in parvalbumin interneurons during hippocampal sharp waves.* Neuron, 2014. **82**(4): p. 908-24.

27. Antic, S.D., M. Hines, and W.W. Lytton, *Embedded ensemble encoding hypothesis: The role of the "Prepared" cell.* J Neurosci Res, 2018. **96**(9): p. 1543-1559.

28. Antic, S.D., *Action potentials in basal and oblique dendrites of rat neocortical pyramidal neurons.* J Physiol, 2003. **550**(1): p. 35-50.

29. Zhou, W.L., P. Yan, J.P. Wuskell, L.M. Loew, and S.D. Antic, *Intracellular long wavelength voltage-sensitive dyes for studying the dynamics of action potentials in axons and thin dendrites.* Journal of Neuroscience Methods, 2007. **164**(2): p. 225-39.

30. Hines, M.L. and N.T. Carnevale, *The NEURON simulation environment.* Neural Computation, 1997. **9**(6): p. 1179-209.

31. Acker, C.D. and S.D. Antic, *Quantitative assessment of the distributions of membrane conductances involved in action potential backpropagation along basal dendrites.* J Neurophysiol, 2009. **101**(3): p. 1524-41.

32. Mainen, Z.F., N.T. Carnevale, A.M. Zador, B.J. Claiborne, and T.H. Brown, *Electrotonic architecture of hippocampal CA1 pyramidal neurons based on three-dimensional reconstructions.* Journal of Neurophysiology, 1996. **76**(3): p. 1904-23.

33. Migliore, M., D.A. Hoffman, J.C. Magee, and D. Johnston, *Role of an A-type K+ conductance in the back-propagation of action potentials in the dendrites of hippocampal pyramidal neurons.* Journal of Computational Neuroscience, 1999. **7**(1): p. 5-15.

34. Kampa, B.M. and G.J. Stuart, *Calcium spikes in basal dendrites of layer 5 pyramidal neurons during action potential bursts.* J Neurosci, 2006. **26**(28): p. 7424-32.

35. Kole, M.H., S. Hallermann, and G.J. Stuart, *Single Ih channels in pyramidal neuron dendrites: properties, distribution, and impact on action potential output.* J Neurosci, 2006. **26**(6): p. 1677-87.

36. Stadler, K., C. Bierwirth, L. Stoenica, A. Battefeld, O. Reetz, E. Mix, S. Schuchmann, T. Velmans, K. Rosenberger, A.U. Brauer, S. Lehnardt, R. Nitsch, M. Budt, T. Wolff, M.H. Kole, and U. Strauss, *Elevation in type I interferons inhibits HCN1 and slows cortical neuronal oscillations.* Cereb Cortex, 2014. **24**(1): p. 199-210.

37. Reetz, O., K. Stadler, and U. Strauss, *Protein kinase C activation mediates interferon-beta-induced neuronal excitability changes in neocortical pyramidal neurons.* J Neuroinflammation, 2014. **11**: p. 185.

38. Destexhe, A., Z.F. Mainen, and T.J. Sejnowski, *Synthesis of models for excitable membranes, synaptic transmission and neuromodulation using a common kinetic formalism.* Journal of Computational Neuroscience, 1994. **1**(3): p. 195-230.

39. Schiller, J., G. Major, H.J. Koester, and Y. Schiller, *NMDA spikes in basal dendrites of cortical pyramidal neurons.* Nature, 2000. **404**(6775): p. 285-9.

40. Milojkovic, B.A., J.P. Wuskell, L.M. Loew, and S.D. Antic, *Initiation of sodium spikelets in basal dendrites of neocortical pyramidal neurons.* J Membr Biol, 2005. **208**(2): p. 155-69.

41. Goldstein, S.S. and W. Rall, *Changes of action potential shape and velocity for changing core conductor geometry.* Biophysical Journal, 1974. **14**(10): p. 731-57.

42. Moore, J.W. and M. Westerfield, *Action potential propagation and threshold parameters in inhomogeneous regions of squid axons.* J Physiol, 1983. **336**: p. 285-300.

43. Arnth-Jensen, N., D. Jabaudon, and M. Scanziani, *Cooperation between independent hippocampal synapses is controlled by glutamate uptake.* Nat Neurosci, 2002. **5**(4): p. 325-31.

44. Scimemi, A., A. Fine, D.M. Kullmann, and D.A. Rusakov, *NR2B-containing receptors mediate cross talk among hippocampal synapses.* J Neurosci, 2004. **24**(20): p. 4767-77.

45. Chalifoux, J.R. and A.G. Carter, *Glutamate spillover promotes the generation of NMDA spikes.* J Neurosci, 2011. **31**(45): p. 16435-46.

46. Oikonomou, K.D., S.M. Short, M.T. Rich, and S.D. Antic, *Extrasynaptic glutamate receptor activation as cellular bases for dynamic range compression in pyramidal neurons.* Front Physiol, 2012. **3**: p. 334.

47. Losonczy, A., J.K. Makara, and J.C. Magee, *Compartmentalized dendritic plasticity and input feature storage in neurons.* Nature, 2008. **452**(7186): p. 436-41.

48. Remy, S., J. Csicsvari, and H. Beck, *Activity-dependent control of neuronal output by local and global dendritic spike attenuation.* Neuron, 2009. **61**(6): p. 906-16.

49. Short, S.M., K.D. Oikonomou, W.L. Zhou, C.D. Acker, M.A. Popovic, D. Zecevic, and S.D. Antic, *The stochastic nature of action potential backpropagation in apical tuft dendrites.* J Neurophysiol, 2017. **118**(2): p. 1394-1414.

50. Larkum, M.E. and T. Nevian, *Synaptic clustering by dendritic signalling mechanisms.* Curr Opin Neurobiol, 2008. **18**(3): p. 321-31.

51. Wilson, D.E., D.E. Whitney, B. Scholl, and D. Fitzpatrick, *Orientation selectivity and the functional clustering of synaptic inputs in primary visual cortex.* Nat Neurosci, 2016. **19**(8): p. 1003-9.

52. Carmignoto, G. and T. Fellin, *Glutamate release from astrocytes as a non-synaptic mechanism for neuronal synchronization in the hippocampus.* J Physiol Paris, 2006. **99**(2-3): p. 98-102.

53. Rusakov, D.A. and D.M. Kullmann, *Extrasynaptic glutamate diffusion in the hippocampus: ultrastructural constraints, uptake, and receptor activation.* J Neurosci, 1998. **18**(9): p. 3158-70.

54. Tovar, K.R. and G.L. Westbrook, *The incorporation of NMDA receptors with a distinct subunit composition at nascent hippocampal synapses in vitro.* J Neurosci, 1999. **19**(10): p. 4180-8.

55. Harris, A.Z. and D.L. Pettit, *Extrasynaptic and synaptic NMDA receptors form stable and uniform pools in rat hippocampal slices.* J Physiol, 2007. **584**(Pt 2): p. 509-19.

56. De-Miguel, F.F. and K. Fuxe, *Extrasynaptic neurotransmission as a way of modulating neuronal functions.* Front Physiol, 2012. **3**: p. 16.

57. Petralia, R.S., *Distribution of extrasynaptic NMDA receptors on neurons.* ScientificWorldJournal, 2012. **2012**: p. 267120.

58. Petralia, R.S., Y.X. Wang, F. Hua, Z. Yi, A. Zhou, L. Ge, F.A. Stephenson, and R.J. Wenthold, *Organization of NMDA receptors at extrasynaptic locations.* Neuroscience, 2010. **167**(1): p. 68-87.

59. Papouin, T. and S.H. Oliet, *Organization, control and function of extrasynaptic NMDA receptors.* Philos Trans R Soc Lond B Biol Sci, 2014. **369**(1654): p. 20130601.

60. Wei, D.S., Y.A. Mei, A. Bagal, J.P. Kao, S.M. Thompson, and C.M. Tang, *Compartmentalized and binary behavior of terminal dendrites in hippocampal pyramidal neurons.* Science, 2001. **293**(5538): p. 2272-5.

61. Cai, X., C.W. Liang, S. Muralidharan, J.P. Kao, C.M. Tang, and S.M. Thompson, *Unique roles of SK and Kv4.2 potassium channels in dendritic integration.* Neuron, 2004. **44**(2): p. 351-64.

62. Milojkovic, B.A., W.L. Zhou, and S.D. Antic, *Voltage and Calcium Transients in Basal Dendrites of the Rat Prefrontal Cortex.* J Physiol, 2007. **585**(2): p. 447-468.

63. Kampa, B.M., J.J. Letzkus, and G.J. Stuart, *Requirement of dendritic calcium spikes for induction of spike-timing-dependent synaptic plasticity.* J Physiol, 2006. **574**(Pt 1): p. 283-90.

64. Hodgkin, A.L. and A.F. Huxley, *A quantitative description of membrane current and its application to conduction and excitation in nerve. 1952 [classical article]. [Review] [16 refs].* Bulletin of Mathematical Biology, 1990. **52**(1-2): p. 25-71.

65. Wickens, J.R. and C.J. Wilson, *Regulation of action-potential firing in spiny neurons of the rat neostriatum in vivo.* J Neurophysiol, 1998. **79**(5): p. 2358-64.

66. Azouz, R. and C.M. Gray, *Dynamic spike threshold reveals a mechanism for synaptic coincidence detection in cortical neurons in vivo.* Proc Natl Acad Sci U S A, 2000. **97**(14): p. 8110-5.

67. Neymotin, S.A., B.A. Suter, S. Dura-Bernal, G.M. Shepherd, M. Migliore, and W.W. Lytton, *Optimizing computer models of corticospinal neurons to replicate in vitro dynamics.* J Neurophysiol, 2017. **117**(1): p. 148-162.

68. Dura-Bernal, S., S.A. Neymotin, B.A. Suter, G.M. Shepherd, and W.W. Lytton, *Long-range inputs and H-current regulate different modes of operation in a multiscale model of mouse M1 microcircuits.* bioRxiv., 2018. **2018**(201707).

*

Fig 1 – Dendritic Voltage Waveforms

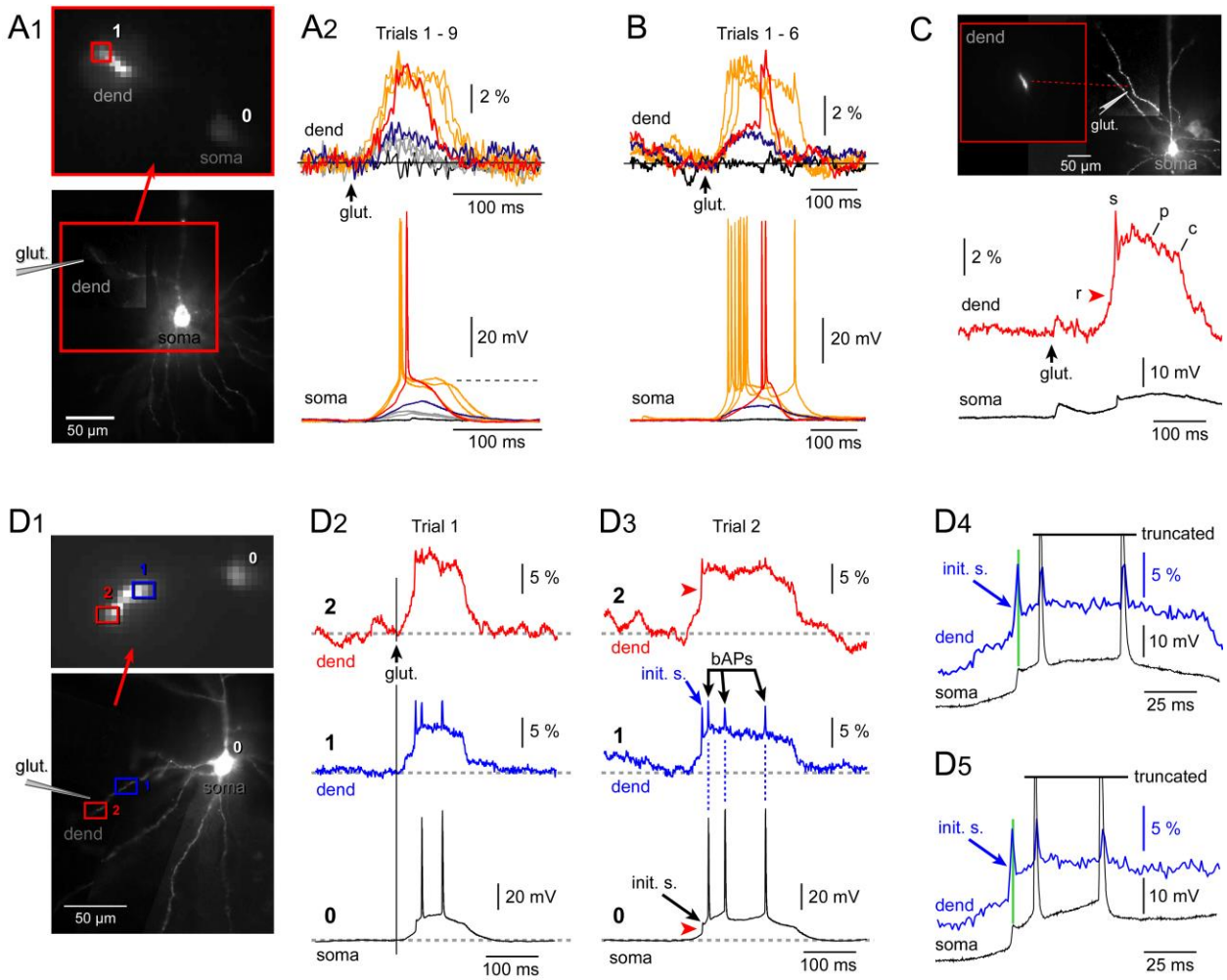

Figure 1. Voltage waveforms of the glutamate evoked dendritic plateau potentials.
(A_1) Pyramidal neuron filled with JPW-3028. Area inside rectangle is imaged at 2.7 kHz. Only one dendrite is illuminated by laser spot. **(A_2)** Glutamate was applied iontophoretically at location indicated in *A_1*. The intensity of the glutamatergic stimulation was increased in equal steps through 9 recording trials (Trials 1-9), while optical signals were recorded in the dendritic region of interest (ROI) marked by the red rectangle. "Soma" marks the somatic whole cell recordings obtained simultaneously with the optical signals. (**B**) Same experimental paradigm as in *A,* except different cell. (**C**) Glutamatergic stimulation of an oblique dendrite (duration 5 ms) triggers a local plateau potential. r-fast rise; s-initial sodium spikelet; p-plateau phase; c-collapse of the plateau. (**D_1**) Pyramidal neuron filled with JPW-3028. The position of the glutamate-filled sharp electrode is marked by drawing. (**D_2**) In Trial 1, glutamate-induced membrane potential changes are recorded simultaneously at two ROIs on the same dendrite and in the cell body (whole-cell). (**D_3**) In Trial 2, the glutamatergic stimulus was increased by 20% causing a longer lasting plateau phase. The initial spikelet in the somatic recordings (black arrow) is caused by the initial spikelet in the dendritic recording (blue arrow). The rapid inflection preceding the plateau phase (red arrowhead) is also present in the somatic whole-cell recordings (red arrowhead). Three backpropagating APs (bAPs) recorded in dendrite are marked by black arrows. (**$D_{4,5}$**) Blowups of *D_2* and *D_3* on faster time scales to show that initial spikelet (init. s.) precedes the somatic kink in both trials.

Fig 2 – Model outline, Backpropagation and Glutamate Spillover

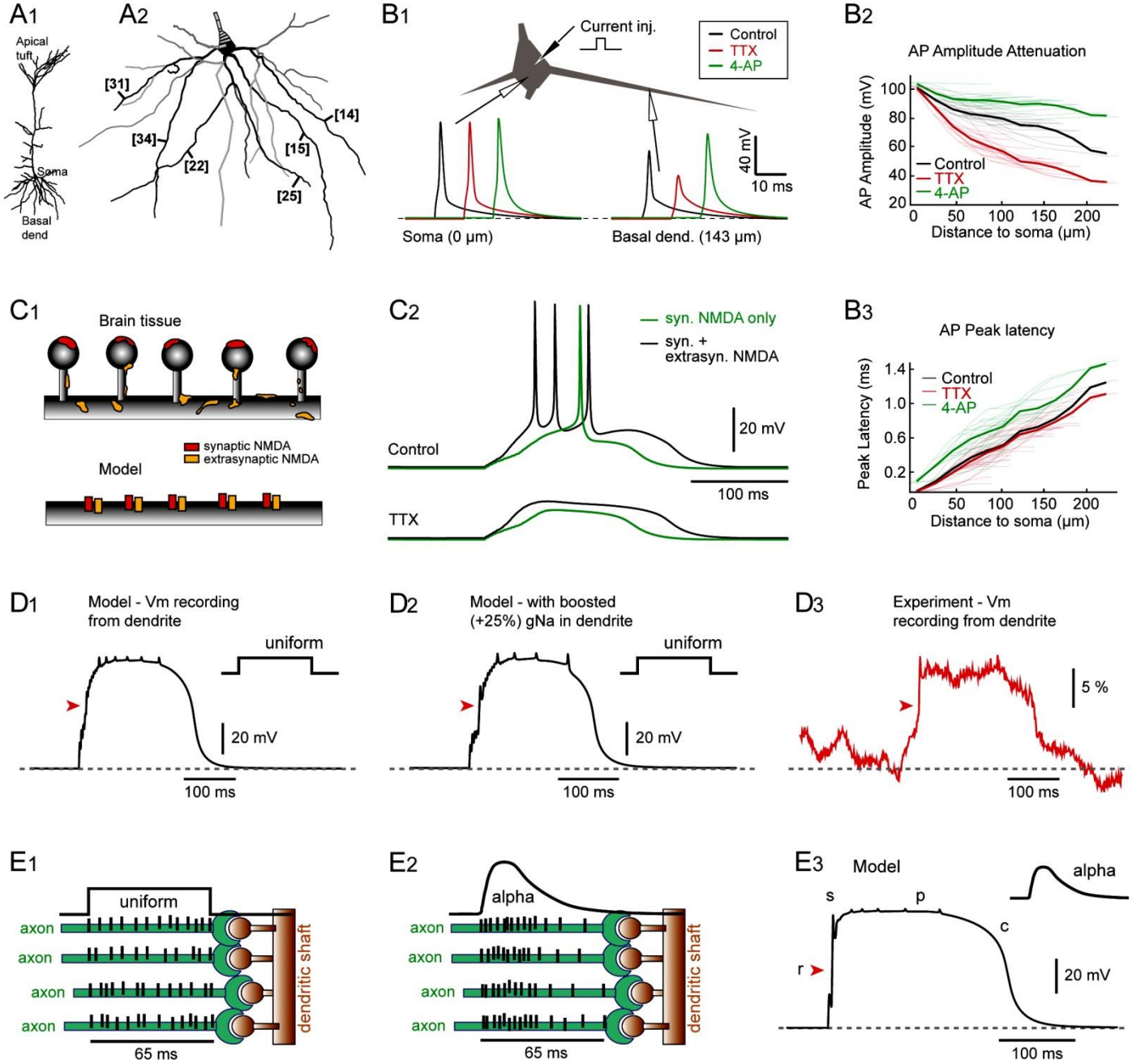

Figure 2. Model outline.

(A_1) Reconstructed pyramidal neuron. **(A_2)** Six basal dendrites, mostly used in data quantifications, are labeled by bracketed numbers. **(B_1)** The bAP amplitude, peak latency, response to TTX and 4-AP match the experimental measurements obtained in basal dendrites using voltage sensitive dyes. ($B_{2,3}$) Quantification of the model results. **(C_1)** Glutamate stimulations activate the AMPA and NMDA receptors on dendritic spines (red) and the NMDA receptors on extrasynaptic surfaces, including the spine head, spine neck, and dendritic shaft (yellow). **(C_2) (upper)** The comparison of simulated traces with and without extrasynaptic NMDARs. Green = Somatic response evoked by synaptic NMDARs only. Black - Somatic response evoked by conjugate activation of both synaptic and extrasynaptic NMDARs. **(lower)** Same traces as in *C_2-upper*, but with the application of TTX to block all voltage-activated sodium channels. **(D_1)** Membrane potential change in basal dendrite during a plateau potential obtained in model cell shown in panel *A*. **(D_2)** Same as in *D_1*, except gNa_bar increased by 25%. **(D_3)** Membrane potential change in basal dendrite obtained by voltage-sensitive dye imaging (*from Fig.1D_3*). **(E_1)** Temporal organization of the glutamatergic inputs – uniform random within time window of 65 ms. Presynaptic axons (green) impinging on dendritic spines (brown). Ticks indicate APs in axon. **(E_2)** Temporal organization of inputs – alpha random function. **(E_3)** Dendritic plateau potential with alpha distribution of inputs. "r", "s", "p", & "c" same definition as in Fig. 1.

Fig 3 – Somatic waveforms, experiments vs. models

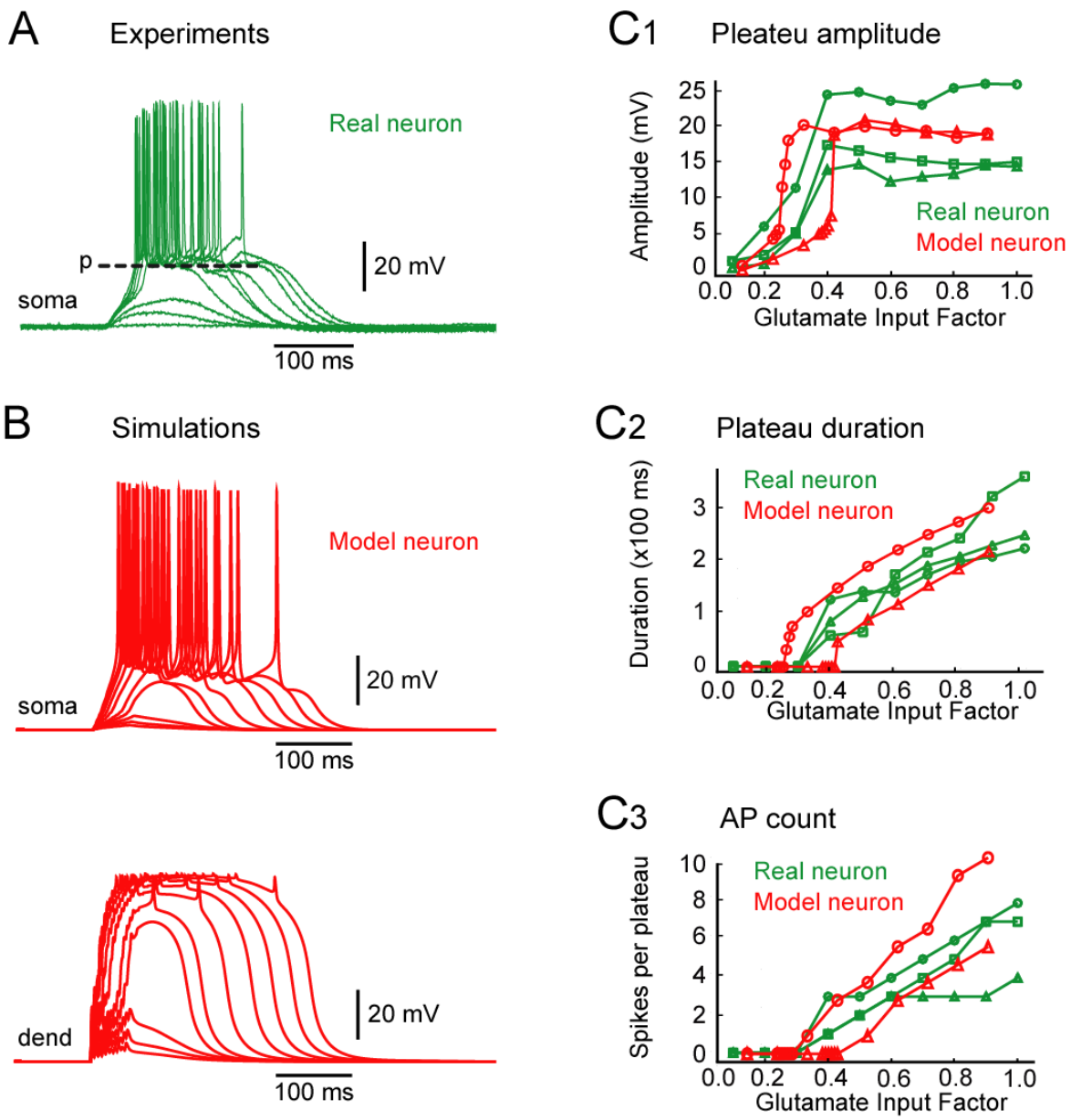

Figure 3. Varying levels of glutamatergic input in experiments and model.
(A) Somatic whole cell recordings in a layer 5 pyramidal neuron. Glutamate microiontophoresis was applied on one basal branch ~90 µm away from the soma. The intensity of the glutamate iontophoretic current was increased gradually in equal steps. **(B)** Computational model of the simultaneous somatic and dendritic voltage recording in response to glutamate application on one basal dendrite. Distance from the soma = 110 µm. The NMDAr mechanism here is based on Destexe et al., 1994 (our Model 1). The Model 2 data (employing the Major et al., 2008 NMDAr mechanism) is shown in **Suppl. Fig. S1B**. **(B)** Dendritic voltage trace obtained from the model basal branch, where glutamate stimulation was applied. **(C_{1-3})** Numerical analysis of the experimental data obtained in 3 real neurons (green) and 2 model neurons (red).

Fig 4 - Plateau duration in soma and dendrite

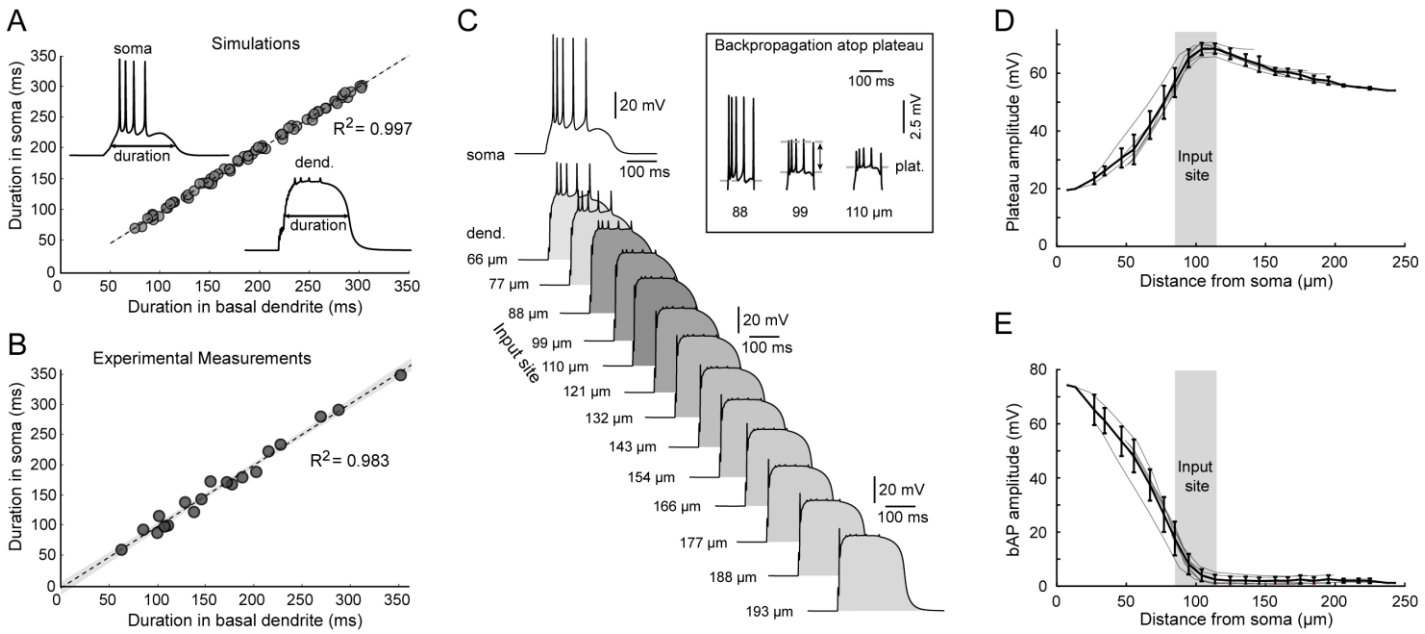

Figure 4. Voltage waveforms in soma and dendrite are strongly correlated.
(A) Comparisons between dendritic and somatic voltage transients obtained in the model simulations. n = 70 sweeps in 6 model basal branches. Insets depict the method used for measuring plateau amplitude and duration in dendrite and soma. **(B)** Experimental measurements in rat brain slices using simultaneous recordings of voltage waveforms in dendrite (voltage imaging) and soma (whole-cell). n = 19 sweeps from 5 pyramidal neurons. Linear fitting by ordinary least squares regression. The 95% confidence interval is marked by gray shading. **(C)** Computer simulation. Dendritic voltage waveforms obtained simultaneously from 13 locations along basal dendrite and cell body (soma). Inset: bAPs emerge from the plateau phase. Horizontal line “p” marks the amplitude of the plateau phase. Two-sided arrow indicates method used for measuring “AP amplitude above plateau”. **(D)** Dendritic plateau amplitude as function of distance from cell body. **(E)** Amplitude of bAPs above plateau level, as function of distance from cell body.

Fig 5 – Input Location

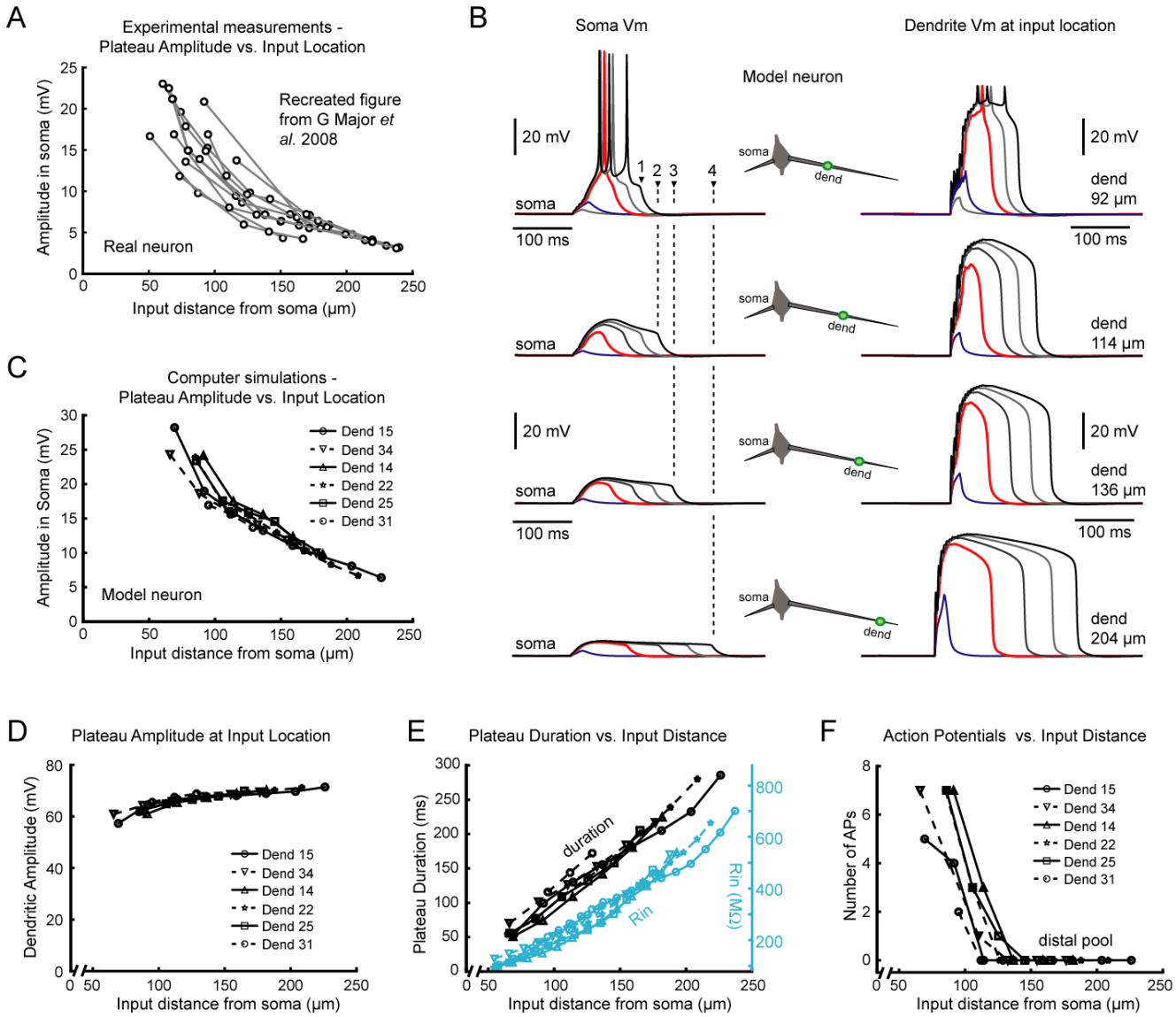

Figure *5*. The impact of the input location.
(A) Glutamate microiontophoresis was delivered on the basal branches at various distances from the cell body and membrane potential changes recorded in the soma. The amplitude of the plateau potential in the soma is plotted against the distance from the cell body – recreated from Major et al., 2008. **(B)** Computer simulation of the experiment described in *A*. Results obtained with our "Model 2" (Major et al., 2008) are displayed – simultaneous voltage waveforms in dendrite (at input location) and soma. The precise locations of the glutamate inputs on basal dendrite are annotated above each dendritic trace and expressed as a distance from the cell body in micrometers. Vertical dashed lines mark 4 different plateau durations obtained by stimulating basal dendrite at 4 locations – fixed glutamate input intensity. The results of Model 1 (utilizing the Destexe et al. (1994) membrane mechanism for NMDAr channels) are shown in **Suppl. Fig. S2B**. **(C)** Same as *A*, except model neuron data quantification. **(D)** The local amplitude of the dendritic plateau, measured at each glutamate stimulation site, is plotted versus the distance of that stimulation site from the cell body. **(E)** The local duration (half-width) of the dendritic plateau at the glutamate stimulation site is plotted as a function of distance from the cell body. Gray data points depict local dendritic R_{in}. **(F)** Distal glutamatergic inputs (distal pool) generate dendritic plateau potentials, which fail to trigger somatic APs.

Fig 6 – Input Resistance and Membrane Time Constant

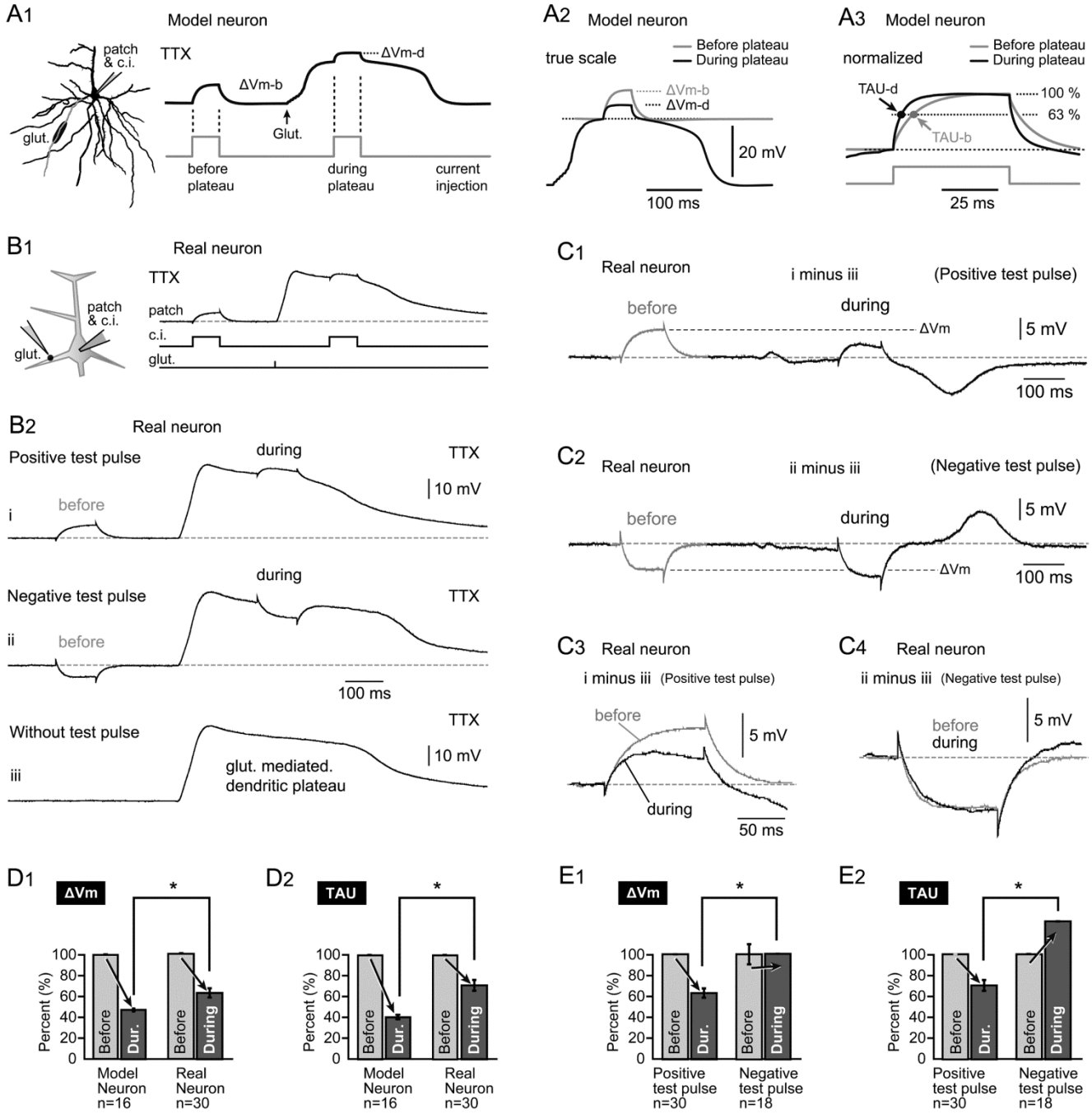

Figure 6. Impact of plateau potentials on the cell body Rin and TAU.
(A_1) Basilar dendritic tree of the model cell. Dendritic segment (66–132 µm) is receiving glutamate inputs. Computer simulation of dendritic plateau potential measured at soma. An identical depolarizing current pulse was injected into the soma before and during the plateau potential (current injection). **(A_2)** Same as in ***A_1***, except, before (black trace) and during (gray trace) are superimposed. (**A_3**) Same as in ***A_2*** except traces are amplitude scaled. **(B_1)** Experimental outline. Whole-cell recordings from cortical L5 pyramidal neuron treated by TTX. Glut. - glutamate pulse (5 ms) was delivered on one basal dendrite (90 µm away from the cell body). Rectangular current pulses (test pulses) were injected into the cell body at two time points, *Before* and *During* glutamate-evoked plateau potential. **(B_2)** Three experimental trials obtained in the same layer 5 pyramidal cell. Experimental paradigm consisted of pairing dendritic plateau potentials with test pulses injected into the cell body. Each trace is an average of 5-7 sweeps obtained from the same cell. **(C_1)** Arithmetic subtraction of traces "i" and "iii" (shown in ***B_2***). **(C_2)** Arithmetic subtraction of traces "ii" and "iii". **(C_{3-4})** Test-pulse-evoked somatic voltage transients are superimposed (same scales). **(D_1)** Relative changes in the amplitude of the test pulse-evoked transients (ΔVm) in model and real neurons. A value obtained during plateau was normalized by the value obtained before plateau onset in the same neuron. **(D_2)** Relative plateau-induced changes in TAU obtained in model and real neurons. A TAU value obtained during plateau was normalized by the TAU value obtained in the same neuron before plateau. **(E_1)** Measurements were obtained in real neurons in brain slices. Mean relative change in the amplitude of ΔVm, depending on the polarity of test pulse (positive vs. negative). **(E_2)** Mean relative change in TAU (induced by plateau), depending on the polarity of the test current. n = number of experimental trials (number of dendrites and number of cells are specified in text).

Fig. 7 – Somatic membrane response depends on the proximity of the dendritic input site

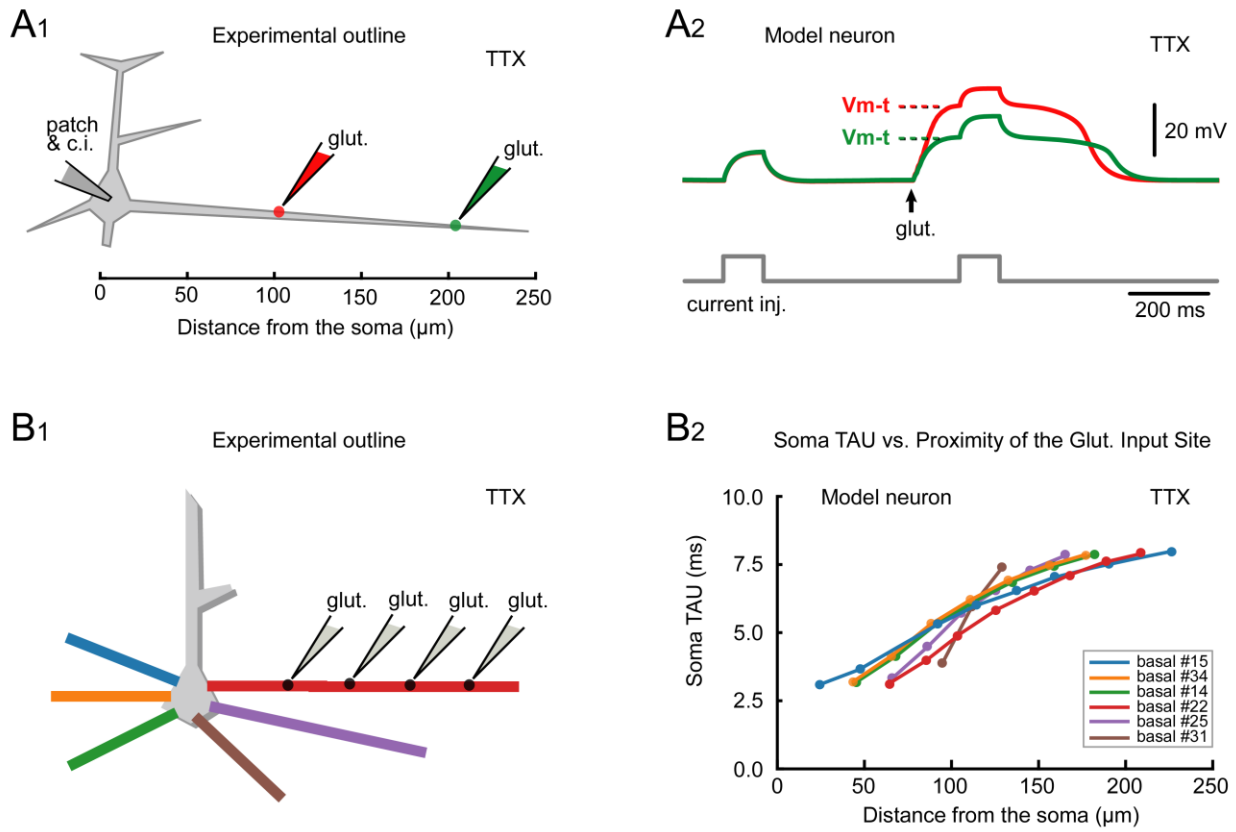

Figure 7. Position of glutamatergic input on basal dendrite determines the plateau-induced changes of soma TAU.
(A_1) In a model cell void of Na^+ channels (to mimic a TTX condition in brain slice experiments), glutamate input of fixed intensity was delivered at two different locations along a basal dendrite. **(A_2)** At a proximal location (red), the amplitude of the glutamate-mediated dendritic plateau potential observed from the cell body (red trace) is greater compared to the same experiment performed at distal dendritic location (green trace). Glutamate-mediated plateau potentials obtained with distal inputs (green trace) last longer than plateaus obtained by more proximal inputs on the same dendrite (red trace). Test pulse was injected into the cell body to test membrane response of the cell body. The membrane charging curve is faster for proximal glutamatergic inputs (red trace). Vm-t marks the membrane voltage at which the test pulse begins. **(B_1)** Data shown in the previous panel suggest dependence of soma TAU on the distance of glutamate input from the soma. To determine if this relation holds in basal dendrites of different morphologies, glutamate input site was shifted along each basal branch. Glutamate location was varied along each branch – input intensity was unchanged. **(B_2)** Quantification of data for experiment shown in B_1. Note that every basal dendrite tested in this model (n=6) showed a similar relation between soma TAU versus the distance at which glutamate input was delivered. Overall, the soma membrane response becomes faster (shorter TAU) if glutamate input is closer to the cell body, regardless of the basal dendrite tested.

Fig 8 – Impact on the AP Initiation

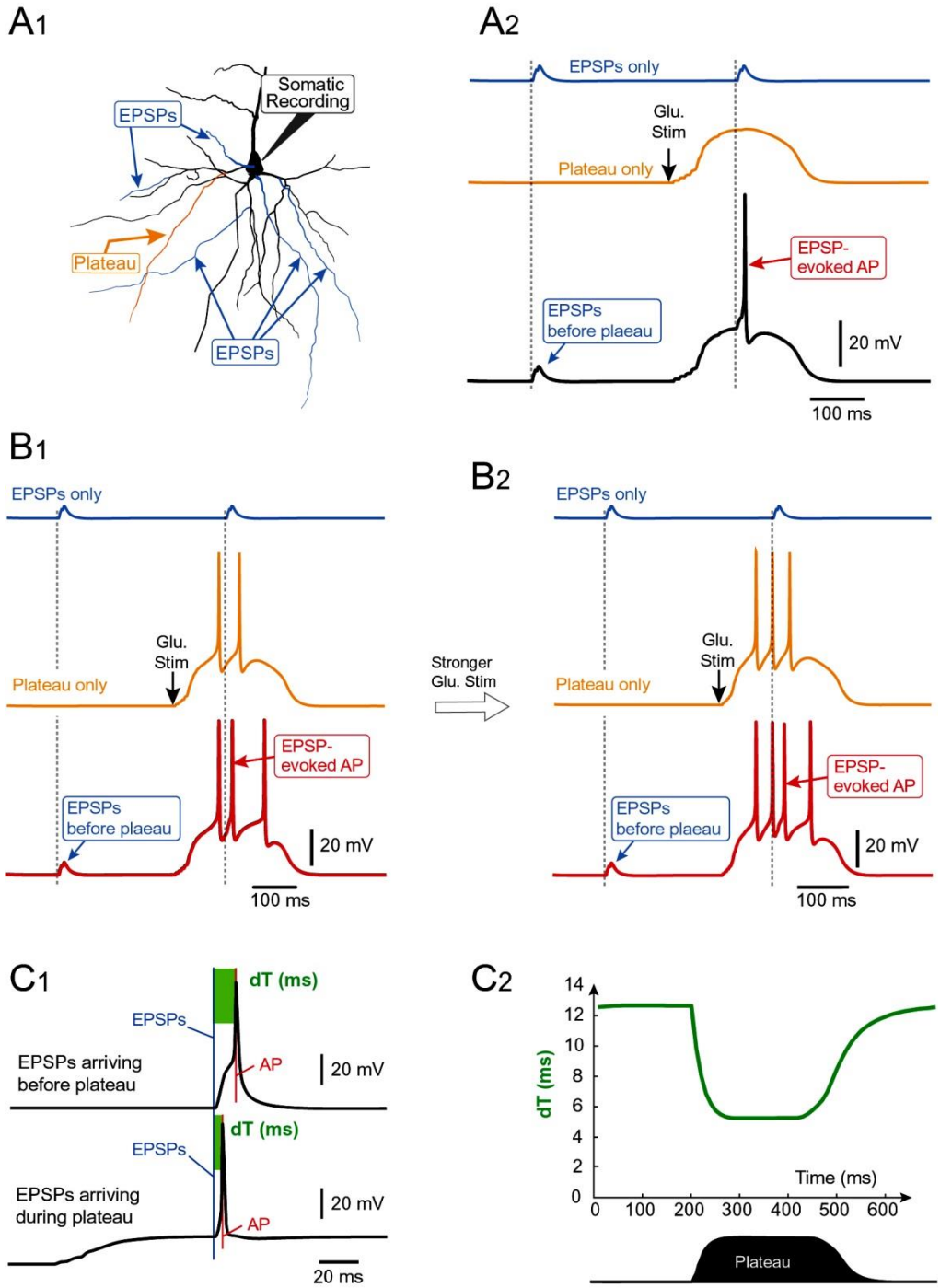

Figure 8. Impact of dendritic plateau potential occurring in one basal dendrite on the integration of EPSPs in other dendrites.
(A_1) Basilar dendritic tree of the model cell. Glutamatergic stimulation for induction of a plateau was delivered onto the branch marked by "plateau". **(A_2)** Blue trace: A barrage of EPSPs (individual EPSPs were received at 5 locations marked by blue arrows in A_1) was delivered on two distinct time points. Orange trace: Glutamatergic stimulation of one basal dendrite produced a somatic plateau subthreshold for axonal AP initiation (spikeless plateau). Black trace: pairing of the stimulation paradigms used in the blue and orange trace. **(B_1)** The same modeling experiment as in A_2, except the EPSP barrages were paired with a stronger plateau potential, accompanied by two APs (spiking plateau). **(B_2)** The same modeling experiment as in B_1, except an even stronger plateau, with more accompanying APs, was used for pairing. **(C_1)** Upper trace: Strong EPSP barrage, capable of triggering AP in the absence of plateau. Lower trace: Pairing of the strong EPSP barrage with a spikeless plateau. Vertical blue line: onset of EPSP barrage. Vertical red line: Peak of the EPSP-evoked AP. Green box: Time delay between the onset of EPSP barrage and the AP peak. **(C_2)** Time delay (dT) is plotted versus the absolute time of the experimental trial (sweep). Initiation of the plateau potential shortens the time delay, dT.